

Design and Development of Smart, Intelligent & IoT Enabled Remote Health Monitoring System

Malyala Pavana Ravi Sai Kiran

A Thesis Submitted to
Indian Institute of Technology Hyderabad
In Partial Fulfillment of the Requirements for
The Degree of Master of Technology



Department of Electrical Engineering

July 2014

Declaration

I declare that this written submission represents my ideas in my own words, and where ideas or words of others have been included, I have adequately cited and referenced the original sources. I also declare that I have adhered to all principles of academic honesty and integrity and have not misrepresented or fabricated or falsified any idea/data/fact/source in my submission. I understand that any violation of the above will be a cause for disciplinary action by the Institute and can also evoke penal action from the sources that have thus not been properly cited, or from whom proper permission has not been taken when needed.



(Signature)

(Malyala Pavana Ravi Sai Kiran)

EE12M1021

(Roll No.)

Approval Sheet

Approval Sheet

This Thesis entitled Design and Development of Smart, Intelligent & IoT Enabled Remote Health Monitoring System by Malyala Pavana Ravi Sai Kiran is approved for the degree of Master of Technology from IIT Hyderabad



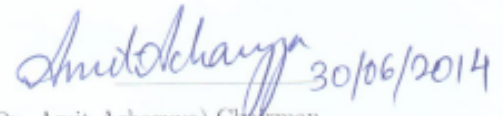
(Dr. Bheemarjuna Reddy Tamma) Examiner
Dept. of Computer Science and Engineering
Indian Institute of Technology Hyderabad



(Dr. Pradeep Kumar Yemula) Examiner
Dept. of Electrical Engineering
Indian Institute of Technology Hyderabad



(Dr. P Rajalakshmi) Adviser
Dept. of Electrical Engineering
Indian Institute of Technology Hyderabad



(Dr. Amit Acharyya) Chairman
Dept. of Electrical Engineering
Indian Institute of Technology Hyderabad

Acknowledgements

The work presented here would not have been possible without the guidance and support of people who in one way or other extended their valuable assistance. I take this opportunity to express my sincere gratitude towards them. First and foremost, I would like to thank my adviser Dr. P Rajalakshmi for her phenomenal valuable guidance and support. Thanks also to Jagadish, and all other people in the WiNet Lab.

Dedication

This work is dedicated to my mother, father and Sneha

Abstract

Drastic developments in the area of Wireless Sensor Networks (WSNs) have paved a path for applications in so called Internet of Things (IoT). Some major applications include remote health monitoring, environment monitoring, smart grids etc. In this work we have identified the primary issues that IoT architectures are facing and developed a system architecture to address the issues identified. IoT architectures primarily face the power constraints due to their battery dependency in remote deployment such as remote health monitoring. Other issue is the hyper connectivity scenario, where the data generated by the sensor networks should have to be limited for efficient management of networks. The proposed architecture consists of an intelligent data transmission mechanism with smart sensing and IEEE 802.15.4 - PHY is considered for communication facility.

The adaptive rule engine based smart transmission proposed transmits the data intelligently thereby reducing the amount of data generated. The important features from the biological data collected are extracted and analyzed for making the decision on the transmission. The proposed smart transmission mechanism aids for a a great reduction in energy consumption and increases the network life time to a great extent. From the analysis made the smart transmission mechanism, reduces the network traffic significantly which also reduces the congestion in network.

The on-chip context predictor based smart sensing also reduces the data generated at the sensor node. It analyses the data collected and calculates the statistical confidence and decides the sampling. It analyses the features present in the data and after achieving a certain confidence interval, it stops sampling thereby reducing the data generated. Thus the over all architecture aids for achieving reduction in duty cycle and energy consumption.

The developed architecture is also equipped with IEEE 802.15.4 - PHY for communication facility. We also discussed the performance of the IEEE 802.15.4 PHY considering BER as key parameter for various pulse shaping techniques. We analysed the tradeoffs to be made in choosing the different pulse shaping techniques.

The performance of the proposed architecture is analyzed using the energy consumption, data rate generated and life time as key parameters. Analysis shoes that the proposed architecture can achieve great energy savings and reduction in network traffic. It also reduces the duty cycle of the system. Hence the proposed architecture can be well suited for IoT remote health monitoring applications under the hyper connectivity scenario.

Contents

Declaration	ii
Approval Sheet	iii
Acknowledgements	iv
Abstract	vi
1 Introduction	1
1.1 Motivation	3
1.2 Outline of the thesis	3
2 Holistic view of System Architecture	4
2.1 12 Lead ECG data conditioning and acquisition system	4
2.2 ECG Feature Extraction	6
2.3 Summary	7
3 Rule engine based smart transmission mechanism	8
3.1 Static Rule engine	8
3.2 Adaptive Rule Engine	10
3.3 Performance Analysis	12
3.3.1 Analysis on Energy Consumption	12
3.3.2 Analysis on Data Rate Generated / Network Load	13
3.3.3 Estimated Battery Lifetime	14
3.4 Summary	14
4 Proposed on-chip context predictor based intelligent sparse sensing and smart transmission architecture	16
4.1 Pre-processing blocks	17
4.2 On-chip context predictor	18
4.3 Performance analysis	18
4.4 Summary	19
5 IEEE 802.15.4-PHY	23
5.1 Performance evaluation of IEEE 802.15.4-PHY without pulse shaping (only DSSS)	24
5.2 Performance evaluation of IEEE 802.15.4-PHY (with DSSS and pulse shaping)	24
5.3 Different Pulse Shaping Techniques	25
5.4 Performance analysis of different pulse shaping techniques	29

5.5	Performance Evaluation of Proposed Modified IEEE 802.15.4-PHY	30
5.6	Summary	30
6	Architecture of the mixer less QPSK modulator system	32
6.1	QPSK modulation	32
6.2	Symbol cycle	34
6.3	Analog bank	35
6.4	Memory	38
6.5	Up/Down counter	38
6.6	Initial state loader	39
6.7	Low pass filter	39
6.8	Performance analysis	39
6.9	Summary	40
7	Conclusion	43
	List of publications	45
	References	45

Chapter 1

Introduction

In remote health monitoring applications, the Body Area Networks (BANs) provide a new paradigm for the Wireless Sensor Networks (WSNs) in monitoring the bio-medical sensors. The data collected by the sensor nodes play a crucial role in further diagnosis. For further diagnosis on the data collected, it has to be transmitted to the central node or gateway node for further processing and storage. In general ZigBee devices which uses the same IEEE 802.15.4 PHY and MAC standard are used for wireless transmission to the central node [1]. In every remote monitoring application, one of the main limitations is power. The sensor nodes that are used to collect data are generally battery powered devices and frequent battery changes are also difficult. In this kind of applications the power consumption by the nodes should be reduced. In the IoT enabled remote health care monitoring applications, the data collected from the sensors should be accessible anytime and anywhere, which requires constant network connectivity. If the remote health care monitoring application, transmits the data continuously, the amount of data generated will be huge. This also contributes to the hyper connectivity scenario. In hyper connectivity each device which has an ability to connect to the network will be connected to the network. According to the predictions made by GSMA, the total number of devices connected will be 15 billion by around 2015 and 24 billion by the year 2020 [9, 10]. Trending development in the Internet of Things (IoT) enabled applications realizes the hyper connectivity scenario much sooner than the predictions. In such cases one of the primary concern relates to the data management. Due to continuous monitoring of the physiological parameters, the amount of data generated is very huge. This huge collection of data results into improper data management in hyper connectivity scenario. In remote health monitoring application we cannot make use of the available bandwidth effectively, if we use the traditional mode of transmitting the data continuously. It even leads to loss of data due to delay and buffer overloading, which is not acceptable particularly in the health care applications. An analysis on the delay and the data loss that occur in the WSNs based on ZigBee technology for transmission due to channel overlapping when the number of nodes that transmit data increase, has been made in [2]. The ZigBee uses only limited number of channels for the transmission. Whenever a ZigBee node has to transfer the data it first performs Clear Channel Assessment (CCA). If the channel is free then the ZigBee node is free to transmit the data to the destination, else the node has to wait for some backoff time which is decided by parameters like Maximum Backoff Number (NB) and Minimum Backoff exponent (BE). A detailed working of the CCA and CSMA-CA in IEEE 802.15.4 standard is given in [1]. As the

amount of data to be transferred increases due to increase in the number of devices, the delay in transmission and losses during the transmission increases.

In order to prevent this scenario, one solution is to reduce the amount of data that is to be transmitted. In remote health monitoring applications the data need not be transferred continuously which will increase load on the network. In the existing architectures for data acquisition and transmission architectures [3], the traditional continuous transmission of data was used, which leads to higher power consumption and increase in the network traffic. In addition computation capabilities in wireless sensors associated embedded systems impose a big challenge in wireless sensor networks. The trade-offs between limited computation and battery power, precision and accuracy of data and delay in discovery of events would need to be balanced and adjusted depending on the applications. Battery may be conserved in different stages of information processing within the systems, from adaptive sampling, processing, to networking and delivery of the data. We have to make sure that the developed processing techniques on the node are low complex and low power for enabling ubiquitous operation of the device.

Many architectures developed mainly aim for conserving power for a particular type of application. For example, an architecture with adaptive sampling algorithm for rare-event detection has the characteristics of sampling more often when an event is likely to happen [4]. This cannot be directly applied to the health monitoring applications as we wish to obtain sensible statistics of the data in the experiments. Moreover, an useful sampling strategy should incorporate data characteristics in the design of the algorithm in order to preserve the features present in the data collected. Similarly many architectures were proposed to achieve low power consumption on IoT scenarios, which cannot be directly adapted to remote health monitoring scenarios.

Recent surveys on Cardiovascular diseases(CVD) risk management, fortified the upsurge of CVDs in developing nations. As a result, Remote health care monitoring broadened for CVD prognosis in care organizations using bulky bedside devices and in addition requirement of medical professionals in operating these devices made the disease prognosis even more critical. Therefore modeling of a robust on chip methodology for cardiac health monitoring is called for, in order to suffice the piling up demand of prognosis centers. In remote health care monitoring the proactive diagnosis is mainly constrained due to the unavailability of the patient under constant monitoring. The primary reasons for this scenario is the user is non-static, which prevents the user from ubiquitous connectivity and the energy consumption of the node. Considering a scenario, where the user is connected to a network using ZigBee which primarily targets for a low data rate and low power applications, the user may go beyond the range ZigBee supports or the battery of the user may die out. In such cases the user loses his connectivity.

Many remote health monitoring procedures were developed in the past such as [5, 6, 7]. In [5], the remote health monitoring system is based on the smart phone for enabling the real time monitoring and full Internet Protocol (IP) connectivity has been used. Primary drawback in this architecture is the excessive power consumption by the smart phones. The battery technology is currently lagging behind the smart phone development. The problems that occur due to the improper data association collected from patients have been discussed in [6]. The architecture proposed in [6] consists of a central gateway which gathers the data from all the users and transfers it to the central server periodically, where clinicians can classify the user's health status. One of the major issues in these remote health monitoring systems is the continuous data transmission, which leads to the hyper

connectivity scenario.

1.1 Motivation

In spite of the large number of studies that proposed many IoT enabled architectures for remote health monitoring, architecture with minimal power consumption under hyper connectivity scenarios is not yet studied in literature. Also most of the previous studies considered either reduction in energy consumption or different methodologies of storage but nevertheless there are any investigations in network traffic reduction by intelligent transmission and smart sensing without loss of any information. Hence the present investigation has been motivated to develop an architecture which can sense minimum amount of data to achieve complete information and transmit the data intelligently thereby guaranteeing no loss in information and confidence of the data.

1.2 Outline of the thesis

The main contribution of this thesis is to offer an architecture for IoT remote health monitoring scenarios, which can achieve a significant energy savings, by reducing the network data rate and system duty cycle. The framework explicitly targets the need for a more efficient way to develop remote health monitoring applications. We especially focus on the minimization of the network energy consumption subject to constraint on data classification. In addition, we consider an ECG remote health monitoring system for all the performance analysis made. The remainder of this chapter is organized as follows. We present an extensive literature survey and present trends in IoT scenario in chapter 1.

In chapter 2, we propose a novel architecture for remote health monitoring applications and we discuss the individual functional units briefly. It includes the ECG data acquisition system developed at IIT Hyderabad.

Chapter 3, discusses the adaptive rule engine based smart transmission and the performance analysis. Performance analysis includes the energy consumption, data rate reduction and life time of the sensor node.

An intelligent on-chip context predictor based smart sensing technique is proposed in chapter 4 and it's performance analysis is discussed.

Chapter 5 discusses the Physical layer of IEEE 802.15.4. It also includes the performance analysis made on the IEEE 802.15.4 - PHY baseband and different pulse shaping techniques. Major tradeoffs that can be made among the different pulse shaping techniques are analysed.

In chapter 6, we developed a mixer less QPSK modulator which can be used for low frequency applications. It includes the hardware prototype developed at IIT Hyderabad and the performance analysis of the developed prototype. Chapter 7 concludes the work by summarizing the study and discussing the future scope.

Chapter 2

Holistic view of System Architecture

The proposed architecture for smart and intelligent remote health monitoring applications is shown in Fig. 2.1. For the analysis of the performance, we consider ECG data acquisition and smart transmission architecture. The architecture can be equally adaptable to any other remote health monitoring application. The architecture primarily focuses on the compressive sensing and smart transmission which aid for low energy consumption. Each of the following functional units present in the architecture are discussed briefly in the subsequent sections.

2.1 12 Lead ECG data conditioning and acquisition system

ECG is a continuous record of voltage changes as a result of physiological changes occurring in the heart muscles. It is usually recorded from the skin using electrodes that are connected to a galvanometer (surface ECG). It can also be recorded by positioning electrodes in the oesophagus in the chambers of heart or directly from myocardium (transesophageal ECG). Surface ECG is the simplest and least expensive technology for diagnosis of cardiac diseases[23]. For performance analysis of the proposed rule engine, a prototype of the ECG data acquisition and signal conditioning system shown in Fig. 2.2, is developed in IIT Hyderabad. The system is used to collect the ECG data from patient using signal processing techniques for removal of the noise generally generated from electrodes contact, body movements and power line. The architecture of the acquisition system is shown in Fig. 2.3. It contains various filtering and amplifying stages. The standard 12 lead ECG acquisition system uses 10 electrodes to collect the 12 Lead ECG data [11]. Recent developments in the ECG data acquisition methodologies made it possible to extract the 12 lead ECG data from 3 lead ECG data [12]. The construction of the 3 lead ECG data acquisition system is easy rather than the standard 12 lead ECG data acquisition system due to the number of electrodes that are to be connected to the body for monitoring of the data. The 3 lead ECG data acquisition system only requires 4 electrodes that are to be connected at 4 different parts of the body. Later the 12 lead ECG data is extracted from the 3 lead ECG data collected. The architecture for the 3 lead ECG data acquisition system is shown in Fig. 2.3. The 3 lead ECG data is collected by using 4 electrodes which are placed on 4 different locations on the body (RA (Right arm), LA (Left arm),

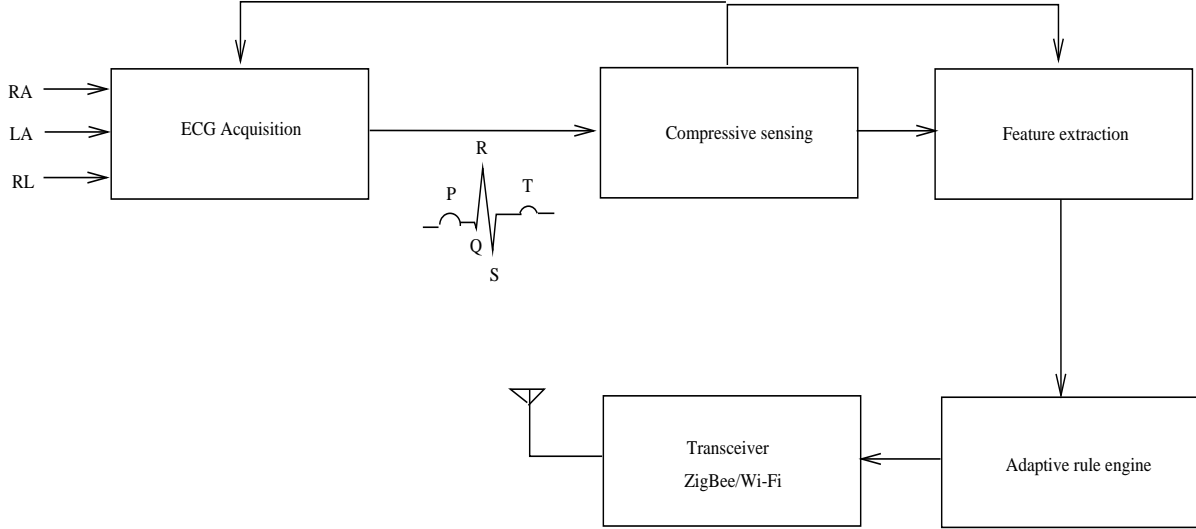


Figure 2.1: Proposed architecture for remote health monitoring system



Figure 2.2: Developed ECG data acquisition system

LL (Left leg), RL (Right leg)). Each lead measures potential difference between two electrodes. For details about the lead's measurement refer to the Table I. The electrode placed in the RL (Right Leg) location is used as the common node for the measurement of the 3 leads.

Case	Lead	Potential diff. between	Common node
1	Lead I	RA & LA	RL
2	Lead II	RA & LL	RL
3	Lead III	LA & LL	RL

Table 2.1: Lead details in 3 Lead ECG data acquisition system

The processing architecture shown in Fig. 2.3 contains an instrumentation amplifier at the beginning and followed by filtering and amplification stages. The lower cut-off frequency is 0.5 Hz and the upper cut-off frequency is 100 Hz. Additionally a notch filter has also been used for removing the power line frequency. Finally for storing the digital data, ADC on the Spartan-3E FPGA is used with a sampling rate of 1000 Hz. A PQRST complex of the lead I from the collected data is shown in Fig. 2.4. The complete analysis followed in this work is made using the lead I ECG data collected from the 9 patients of several age groups collected using the in house developed ECG data acquisition and conditioning system. The same can be applied to the other leads with slight

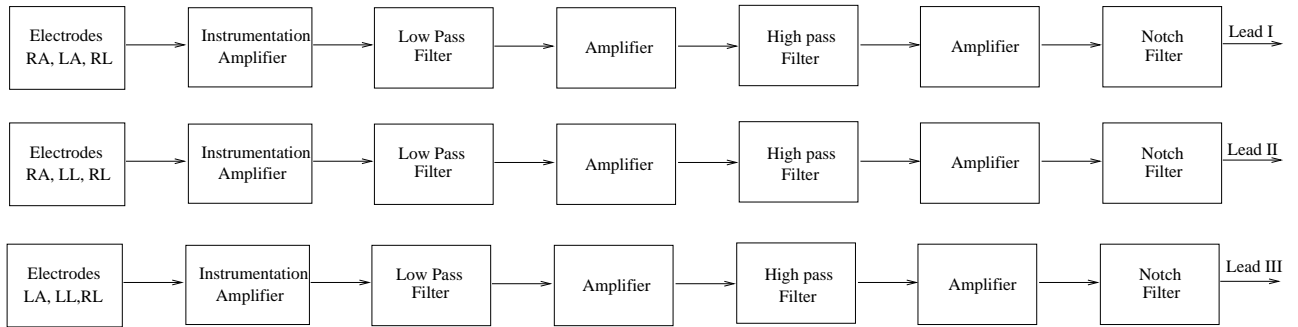


Figure 2.3: 3 Lead ECG Data acquisition architecture

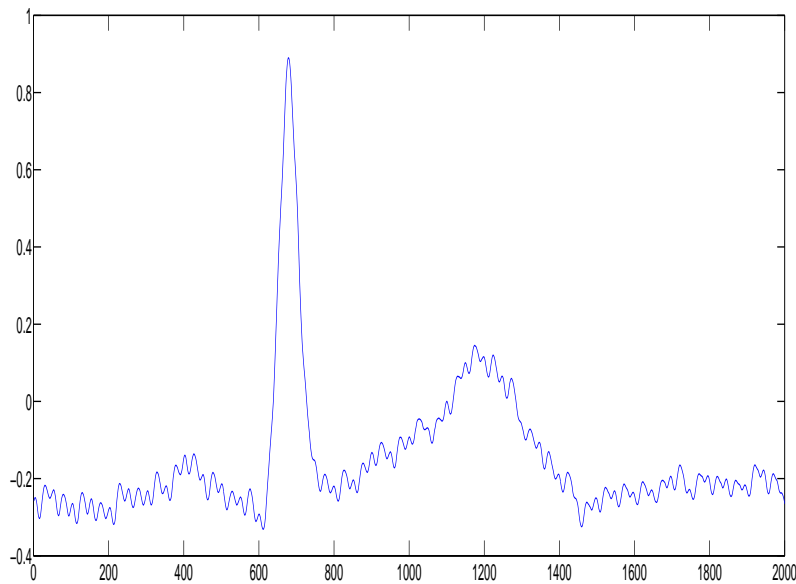


Figure 2.4: PQRST complex from the collected Lead I Digital ECG data

modifications in the architecture.

2.2 ECG Feature Extraction

The present world is equipped technologically providing an automated health prognosis. Usually signals from ECG (Electrocardiogram) are analyzed based on the important features like P, Q, R, S, T as shown in Fig. 5, through which a medical professional annotates to classify the condition of a patient. The P-wave in ECG signal represents atrial depolarization. The QRS depicts the ventricular depolarization. The T-wave gives the atrial and ventricular repolarization [13]. Earlier identifying of these points were based on heuristics. Later on a notion to automate this process, laid foundation for several signal processing algorithms and finally has taken its shape to monitor health of the patient remotely. Identifying these important points by means of some automated algorithms is feature extraction. In recent times there are several feature extraction algorithms

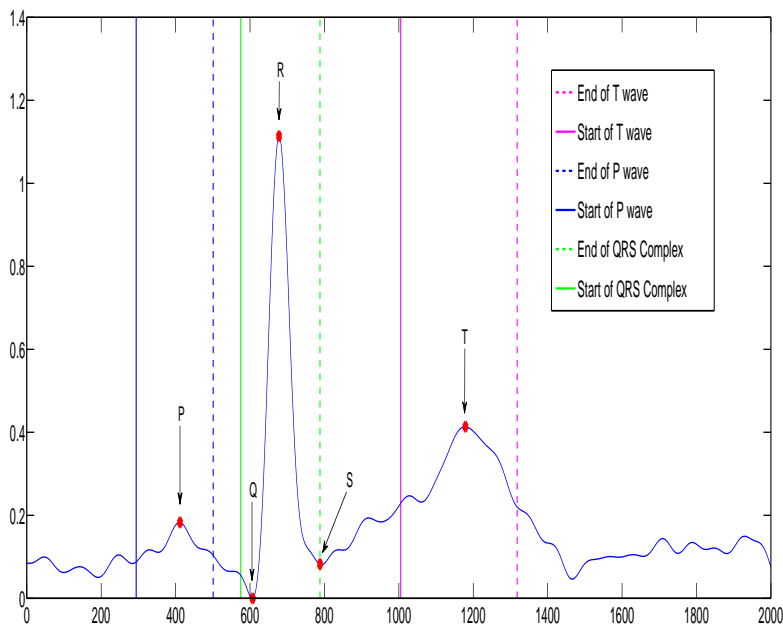


Figure 2.5: Extracted features from Lead-I ECG Data

available [14]-[15]. The state of the art delineation algorithms exploited only R-peak to start with [16]. Then on several other algorithms based on frequency analysis of the ECG signal came into existence with which other points like P, Q, S, T have been eventually identified. It is also essential to have a track on algorithmic accuracy and computational complexity, as in the case of remote health care monitoring the power resources are limited. So further research evolved in developing the low-complex delineation (feature extraction) algorithms [17]-[18] which can be taken as a basis to make classification of the ECG signal. The feature extraction that is used here is based on the wavelet transform with a cascaded filter bank structure. For more detailed working of the feature extraction block, please refer to [17].

The data collected by the acquisition system will be fed to the ECG feature extraction block, which gives us the important features (P, Q, R, S, T) in the data. The features extracted from the data are shown in Fig. 4. Here one can observe the P wave, T wave, QRS Complex. We make use of the intervals calculated from the extracted features in the rule engine to classify the data as normal or abnormal.

2.3 Summary

In this chapter, we discussed the hardware prototype of ECG acquisition system developed in IIT Hyderabad. It has an upper cut-off frequency of 100 Hz and a lower cut-off frequency of 0.5 Hz. The analog ECG acquired is digitized using Spartan 3E FPGA at a sampling rate of 1000 Hz and is stored on local storage. The collected digital ECG signal is then processed using feature extraction block to extract important features such as P, Q, R, S and T points which are the key parameters for doctors in classifying the ECG data.

Chapter 3

Rule engine based smart transmission mechanism

The rule engine is the key component in this architecture, which aids for the low power consumption and the low network traffic generation. Doctors do not need continuous data from the patient which also reduces network efficiency and makes storage a problem. Instead of the continuous transmission of data, one can send the important data which doctors need. The rule engine classifies the data collected upon using the features extracted from the data. It basically consists of two sections namely, *decision making* and *transmitter control* shown in Fig. 6. The decision making section makes use of the features extracted by the feature extraction block. We developed, two types of rule engines and their performances are evaluated based on the data rate they generate and energy consumption.

3.1 Static Rule engine

The static rule engine consists of "*decision making*" section and "*transmitter control*" section. Aim of the decision making section is to analyze the features extracted from the collected data and to decide whether the data is normal or abnormal. The decision made by the decision maker will then be made use by the transmitter control section for controlling the transmitter. The key features that doctors use to classify the data are listed in the Table II. The values listed in the Table II are normal ranges of the ECG data for a healthy patient [8] and are used as the *hard threshold*, which is the bounding limit of perfectly healthy ECG data. If the values of the parameters are in the range listed in the table, the data is then classified as a normal data else it is classified as an abnormal data. Whenever the data is classified as the abnormal data, the rule engine switches on the transmitter and the data samples are transmitted to the gateway. At the same time the samples that are already processed ahead of the current abnormal data and the samples that will be processed after the current data samples are then stored from buffer in to the local storage which resides on the node. The advantage achieved by storing the data is, whenever the doctor is alarmed with the abnormality, the doctor can query and monitor the data that is stored in the local storage during the abnormality. By using this kind of storage mechanism, the accuracy of the diagnosis can be maintained by eliminating false alarms caused sometimes due to the improper contact of the

electrodes. The steps involved in the static rule engine in order to classify the data are given in Algorithm. 1.

Algorithm 1 Static Rule Engine

Initial: Set *HardThreshold* values

```

1: procedure DECISION MAKER(ExtractedFeatures)
2:   Comment: Calculate PR, QRS, QT intervals.
3:   Calculate Data.PR_interval;
4:   Calculate Data.QRS_interval;
5:   Calculate Data.QT_interval;
6:   if Data > HardThreshold then
7:     Decide the patient is abnormal;
8:     CONTROL SECTION(on);
9:     Transmit the data;
10:    Store the data samples in the local storage;
11:  else
12:    Decide the patient is normal;
13:    Do not transmit the data;
14:  end if
15: end procedure
16: procedure CONTROL SECTION(ControlSignal)
17:  if ControlSignal == on then
18:    Switch on the transmitter;
19:    Wait for the data to be transmitted;
20:    Switch off the transmitter;
21:  else
22:    Maintain transmitter in off state;
23:  end if
24: end procedure

```

The features (P, Q, R, S, T) extracted from the lead I ECG data by the feature extraction block are fed to the decision maker section. It then calculates the PR, QRS, QT intervals. The intervals calculated are then compared with the *HardThreshold* values shown in Table. II and makes a decision. If any one of the three intervals calculated exceeds the threshold value, the data is classified as an abnormal data and triggers the control section to switch on the transmitter. Then the control section takes the control signal given by the decision making section and switches on the transmitter.

Case	Parameter	Normal Threshold
1	PR interval	0.12 - 0.20 Sec
2	QRS interval	≤ 0.12 Sec
3	QT interval	≤ 0.42 Sec

Table 3.1: Threshold values of the intervals

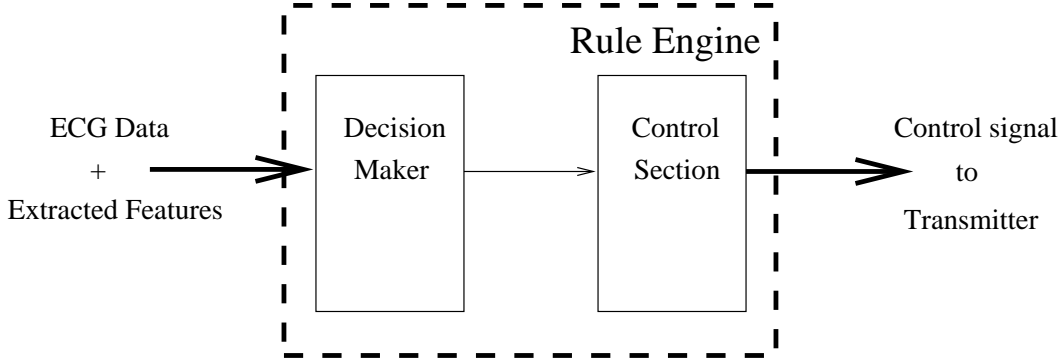


Figure 3.1: Proposed Rule engine

3.2 Adaptive Rule Engine

The static rule engine discussed above uses only a single *hard threshold*, with which it compares the extracted features from the data. It gives a good performance in some situations, but in some situations it performs similar to the traditional continuous transmission architecture. For a patient suffering from first degree atrioventricular block, the PR interval always exceed 0.20 seconds, in this case the data exceeds *hard threshold* always and leads to continuous transmission of the data. It can be better optimized using this adaptive rule engine. Doctors need not be informed every time, the patient crosses the *hard threshold*. In the adaptive rule engine, we make use of two thresholds, *hard threshold* and *soft threshold*. The *hard threshold* is similar to the threshold used in the static rule engine scenario and uses the same threshold values as shown in Table. II. The *soft threshold* is an internal variable, which is initialized to *hard threshold* and whenever the sensed value exceeds the current *soft threshold*, the sensed value is assigned to the *soft threshold*. Steps involved in the adaptive rule engine are shown in ALGORITHM 2.

The input to the adaptive rule engine is same as the static rule engine i.e. the features extracted from the ECG data. Initially the *SoftThreshold* value is same as the *HardThreshold*. Later the values of the *SoftThreshold* parameters are changed based on the observed parameters of the data. In the first iteration, the parameters observed from the data are compared with the *HardThreshold* values. If any of the parameter exceeds, it is classified as an abnormal data and it is again compared with the *SoftThreshold*. In the first iteration the values of the parameters in *SoftThreshold* and *HardThreshold* are same. Hence the parameters also exceed *SoftThreshold*, if they exceed *HardThreshold*. Then the parameter values in which the data exceeded are assigned to the *SoftThreshold* parameters i.e. if in a case the data of a patient has a QRS interval of 0.14 seconds, it will be classified as an abnormal data by the static rule engine. The same will be the case in the first iteration of the adaptive rule engine. Now in the adaptive rule engine, the parameter QRS interval value is changed to 0.14 seconds. In the second iteration, if the same case is repeated, the data will be classified as the abnormal data and the value of the *abnormal_count* value is incremented but the data will not be transmitted. The value *abnormal_count* is used to determine the number of times the patient has crossed the *HardThreshold* but is within the particular *SoftThreshold*. If in the third iteration the data exceeds the QT interval threshold, again the parameter QT interval in the *Soft Threshold* values are adjusted accordingly. The parameter *T* indicates the time to reset the *soft threshold*,

Algorithm 2 Adaptive Rule Engine

Initial: Set *HardThreshold* values
Set *SoftThreshold* = *HardThreshold*
Set *abnormal_count*=0 and start timer *T*;

- 1: **procedure** DECISION MAKER(*ExtractedFeatures*)
- 2: **Comment:** Calculate PR, QRS, QT intervals.
- 3: Calculate *Data.PR_interval*;
- 4: Calculate *Data.QRS_interval*;
- 5: Calculate *Data.QT_interval*;
- 6: **if** *T* expires **then**
- 7: Reset *SoftThreshold*; Restart timer *T*;
- 8: **end if**
- 9: Decide the data is abnormal;
- 10: **if** *Data* > *HardThreshold* **then**
- 11: Decide the data is abnormal;
- 12: Store the data in local storage;
- 13: **if** *Data* > *SoftThreshold* **then**
- 14: CONTROL SECTION(on);
- 15: Transmit the data;
- 16: **if** abnormal *Data.PR_interval* **then**
- 17: *SoftThreshold.PR_interval*=
- 18: *Data.PR_interval*;
- 19: **else if** abnormal *Data.QRS_interval* **then**
- 20: *SoftThreshold.QRS_interval*=
- 21: *Data.QRS_interval*;
- 22: **else if** abnormal *Data.QT_interval* **then**
- 23: *SoftThreshold.QT_interval*=
- 24: *Data.QT_interval*;
- 25: **end if**
- 26: Set *abnormal_count*=0;
- 27: **else**
- 28: Do not change *SoftThreshold* parameters;
- 29: *abnormal_count* = *abnormal_count*+1;
- 30: **end if**
- 31: **else**
- 32: Decide the patient is normal;
- 33: Do not transmit the data;
- 34: **end if**
- 35: **end procedure**
- 36: **procedure** CONTROL SECTION(*ControlSignal*)
- 37: **if** *ControlSignal* == on **then**
- 38: Switch on the transmitter;
- 39: Wait for the data to be transmitted;
- 40: Switch off the transmitter;
- 41: **else**
- 42: Maintain transmitter in off state;
- 43: **end if**
- 44: **end procedure**

Parameter	Initial values		Iteration 1			Iteration 2			Iteration 3		
	Hard threshold (Sec)	Soft threshold (Sec)	Observed value	Hard threshold (Sec)	Soft threshold (Sec)	Observed value	Hard threshold (Sec)	Soft threshold (Sec)	Observed value	Hard threshold (Sec)	Soft threshold (Sec)
PR Interval	0.12 - 0.20	0.12 - 0.20	0.21	0.12 - 0.20	0.12 - 0.21	0.21	0.12 - 0.20	0.12 - 0.21	0.22	0.12 - 0.20	0.12 - 0.22
QRS Interval	0.12	0.12	0.11	0.12	0.12	0.12	0.12	0.12	0.11	0.12	0.12
QT Interval	0.42	0.42	0.41	0.42	0.42	0.40	0.41	0.41	0.42	0.41	0.42
			Abnormality = Yes			Abnormality = Yes			Abnormality = Yes		
			Data transmitted			Data not transmitted, Stored to on board memory			Data transmitted		

Table 3.2: Flow of generic adaptive rule engine for 3 iterations in ECG monitoring

which can be defined by the doctor. After every T duration the *soft threshold* is reset to the *hard threshold* value. If T is set to zero, the adaptive rule engine works similar to the static rule engine.

Table 3.2, depicts the flow of generic adaptive rule engine with ECG monitoring for 3 iterations. The system is assumed to continuously collect sets (1 set = 30 seconds duration) of ECG data. Observed data is the average of features collected within a single set of data. In iteration 1, the observed value of PR interval is 0.21 which exceeds both the *hard threshold* and *soft threshold*. Hence the data is transmitted and *soft threshold* is adjusted accordingly. In iteration 2, the observed value of PR interval exceeds *hard threshold* but does not exceed *soft threshold*. Hence the data is not transmitted but stored onto on board storage thereby guaranteeing no loss of data. The rest of the iterations work in similar fashion. After a particular number of iterations (10 in this case), *soft threshold* is again reset to *Hard threshold*.

3.3 Performance Analysis

The performance analysis of the proposed rule engine is done on the lead I ECG data collected from 9 patients for a duration of 30 seconds at a sampling rate of 1000 Hz, using the in house developed data acquisition system at IIT Hyderabad. Performance metrics that are used in evaluating are energy consumption and the data rate generated. The performance of the proposed rule engine is discussed briefly in the following sections.

3.3.1 Analysis on Energy Consumption

Analytic models for energy consumption of the sensor nodes are done in [19, 22]. In the analysis, they have considered energy consumed by the processor, transceiver and sensors. Here we are considering only the energy consumed by the transmitter as the other parameters remain constant for the analysis. For the modeling of energy consumption, the transmitter is assumed to operate only in two states, on and off state. The energy consumed by the transmitter can be modeled as the energy consumed in a particular state and for the state transitions.

$$E_{cons} = E_{state} + E_{trans} \quad (3.1)$$

$$E_{state} = \sum_i \frac{P_{TX} L_i}{R} + P_{off} T_{off} \quad (3.2)$$

$$E_{trans} = \sum_{j=1}^n P_{on-off} T_{on-off} + \sum_{k=1}^n P_{off-on} T_{off-on} \quad (3.3)$$

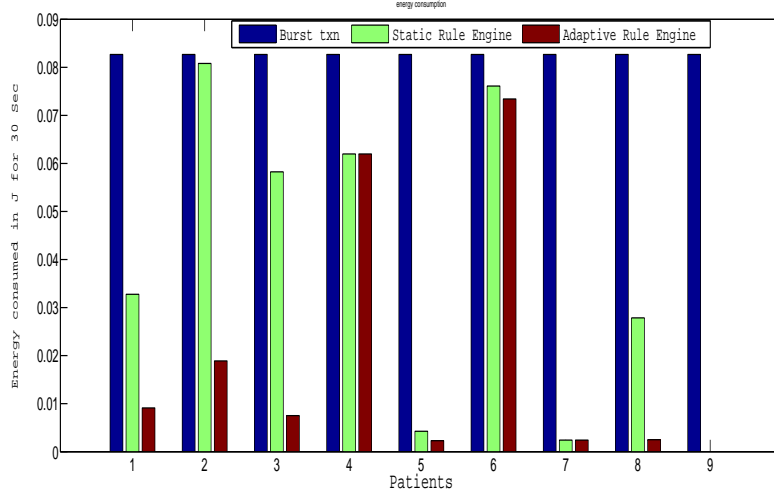


Figure 3.2: Energy consumption in all the three scenarios

For the purpose of analysis, the transmitter is assumed to operate at at 3.3 volts, consume 17 mA current in the transmitting state and $0.02 \mu\text{A}$ in the off state. The E_{cons} in (1) shows the over all power consumption by the transmitter. It is the sum of power consumed in the two states (on, off) and energy consumed for state transitions (on to off, off to on) by the transmitter. The P_{TX} and P_{off} indicates the power consumption in transmitting and off state respectively. T_{off} is the total time the transmitter spent in the off state. L_i indicates the packet length to be transmitted and i indicates the packet number. P_{on-off} and P_{off-on} indicates the power consumed during the state transition from on to off and off to on respectively and the corresponding transition times are T_{on-off} and T_{off-on} . Fig. 3.2 plots Energy consumed by a patient node for transmitting Vs. patient id in three scenarios - burst/continuous transmission, with static rule engine and with adaptive rule engine. In the Fig. 3.2, one can observe the energy consumed using continuous transmission for patient 1 is 0.085 J which is constant for all patients. The power consumed for patient 1, in the static rule engine and adaptive rule engine based transmissions are 0.032 J and 0.008 J respectively. The performance of the adaptive rule engine based transmission is good compared to the other two scenarios. In the case of patient 2, the energy consumed in the static rule engine is 0.078 J, which is nearly same as in the continuous transmission. The reason is, patient 2 is abnormal which leads his ECG data to exceed the hard threshold in most of the cases. In the case of patient 2 the adaptive rule engine performs well by consuming an energy of 0.018 J in 30 seconds. In the case of patient 9, the ECG data observed is normal all the time, which leads static rule engine and adaptive rule engine behave in the same way. From Fig. 7, we can observe that the proposed adaptive rule engine yields significant energy saving compared to the other two scenarios.

3.3.2 Analysis on Data Rate Generated / Network Load

Fig. 3.3 plots the data rate generated per patient Vs. the patient id. The data rate generated depends on the number of abnormal samples, that have to be transmitted. Each sample is encoded using 12 bits symbol. From Fig. 3.3, it is observed that the continuous transmission transmission

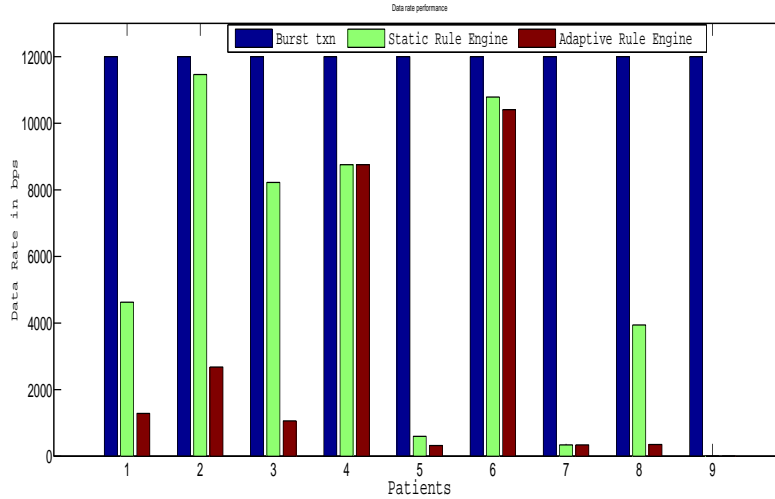


Figure 3.3: Data rate generated in all the three scenarios

for patient 1, leads to a data rate of 12 K bps and remains constant for all the patients, whereas the adaptive rule engine generates a data rate of 1.6 K bps. The expected delay and losses in the burst transmission scenario will be high compared to the static rule engine and adaptive rule engine scenarios. Thus by using the adaptive rule engine based transmission, the network traffic can be significantly reduced compared to the other two scenarios.

3.3.3 Estimated Battery Lifetime

For the estimation of the battery life time, a 3.3 volt, 2300 mAh battery is considered. Fig. 3.4 plots the estimated life time of the battery Vs. patient id. For patient 9 the energy consumed is very less compared to other 8 patients, since he is a normal person there is no much data to be transmitted. The battery life time of the patient 9 is very high. For scaling purposes the patient 9 is not included in the figure. For estimating battery life, power consumed by the patient in the 30 seconds interval is considered as an average power consumption. In the Fig. 3.4, one can observe that the battery life time in the adaptive rule engine based transmission scenario is far better than the burst scenario in most of the cases. In the case of patient 5 the battery can last for upto 11.4 years in adaptive rule engine based transmission scenario compared to 0.314 years in the burst transmission scenario.

The analysis shown above is also performed using the ECG data from "The PTB Diagnostic ECG Database" data base [20]-[21], which also yielded the similar performance.

3.4 Summary

In this chapter, we proposed an rule engine based smart transmission mechanism. Two kinds of rule engines: static rule engine and adaptive rule engine were proposed and their performance is evaluated. For the performance evaluation, ECG data of different patients of different age groups were considered. The analysis show that the adaptive rule engine based transmission mechanism gives better performance by achieving very good energy savings and significant reduction in the

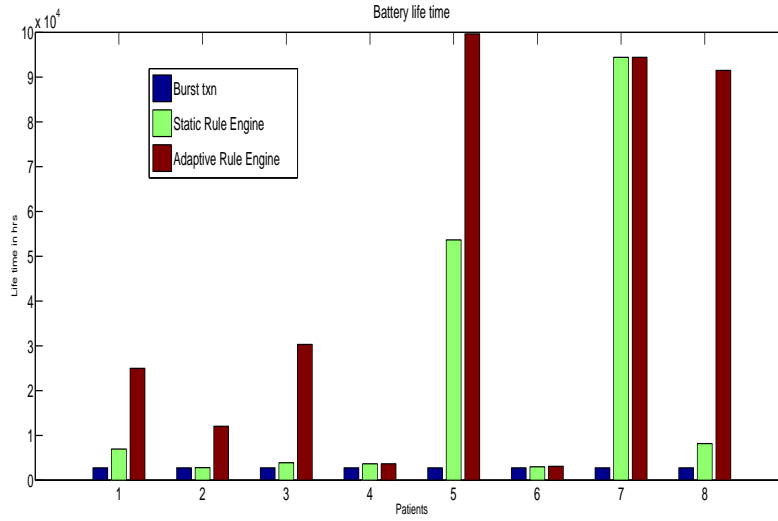


Figure 3.4: Estimated battery life time in all the three scenarios

network traffic generated. The adaptive rule engine based health care data acquisition and smart transmission architecture can aid, low power and low data rate networks, which is an important aspect of IoT enabled health care systems.

Chapter 4

Proposed on-chip context predictor based intelligent sparse sensing and smart transmission architecture

The proposed architecture of on-chip context predictor based intelligent sampling and transmission for remote health monitoring applications is shown in Fig. 6.2. The main idea behind the sparse sampling is to reconstruct the original signal from fewer samples. What is most remarkable about these sampling protocols is that they allow a sensor to very efficiently capture the important information required that is present in a sparse signal [24]. ECG data in general consists of important features such as PR, QRS and QT intervals. The proposed architecture mainly aims to capture these features by collecting minimum amount of samples. Rest of the sections briefly describe the functional units of the proposed on-chip context predictor based intelligent sparse sensing mechanism along with smart transmission.

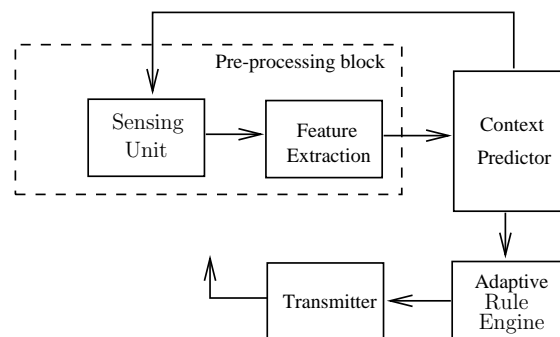


Figure 4.1: Proposed on-chip context predictor based intelligent sparse sensing and smart transmission Architecture

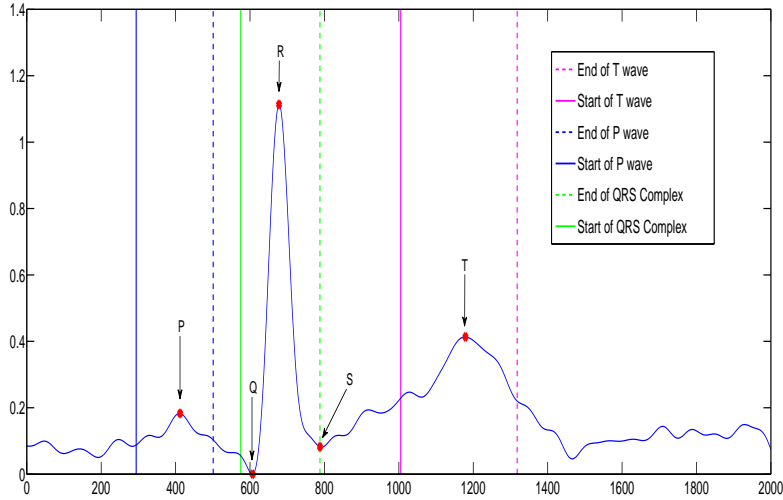


Figure 4.2: PQRST complex from the collected Lead I Digital ECG data

4.1 Pre-processing blocks

The pre-processing block includes the ECG data acquisition unit which acquires the medical data from sensors using noise removal signal processing techniques and feature extraction which extracts the important features from the collected data. Many architectures for the data acquisition system have been developed in the past [25, 11]. For the analysis of performance, Lead I ECG data is considered. The sensing unit which is developed in IIT Hyderabad, has a lower cutoff frequency of 0.5 Hz and an upper cutoff frequency of 120 Hz with a sampling rate of 1000 Hz. Better proactive diagnosis can be given only if the data collected from the patient is classified properly. This intelligent classification can be achieved by extracting important features from the collected data, from which we can discover the abnormalities in the patient. This process of collecting features from the patients physiological data is termed as feature extraction. Feature extraction plays an important role in automating the remote health monitoring. Features like P, Q, R, S and T points shown in Fig. 4.2 from the Lead I ECG signal plays a prominent role in classifying the data collected from the patient. For a detailed description of several feature extraction algorithms available, kindly refer to [15, 17, 14]. Using these extracted features the intervals shown in parameters column of Table 4.1 are calculated and fed to the on-chip context predictor. Table 4.1 shows the important features that are present in ECG signal and their normal threshold values for a healthy patient.

Case	Parameter	Normal Threshold
1	PR interval	0.12 - 0.20 Sec
2	QRS interval	≤ 0.12 Sec
3	QT interval	≤ 0.42 Sec

Table 4.1: Threshold values of the features present in ECG signal

4.2 On-chip context predictor

The on-chip context predictor aids for controlling the sampling rate of sensing unit by predicting the context of the patient. It makes use of the confidence interval calculated over the features extracted from the collected data. If the confidence interval meets the expected threshold it stops sampling, thereby reducing the duty cycle of the system. In [26], Parkin et al. have investigated five methods of calculating confidence intervals (CI) for the mean of a log-normally distributed variable and concluded that the method developed by Land [27] was the best at estimating the lower (LCL) and upper confidence limits (UCL) for small number of samples and are given by

$$LCL = exp \left\{ \bar{\mu} + \frac{\hat{\sigma}^2}{2} + \frac{\hat{\sigma} C_L}{\sqrt{n-1}} \right\} \quad (4.1)$$

$$UCL = exp \left\{ \bar{\mu} + \frac{\hat{\sigma}^2}{2} + \frac{\hat{\sigma} C_U}{\sqrt{n-1}} \right\} \quad (4.2)$$

Where C_L and C_U are H-statistic parameters calculated from a function that depends on the number of observations (n), the standard deviation of the log-transformed values ($\hat{\sigma}$) and the significance level α selected. The values of C_L and C_U used here are based on 98 percentile values of the methods and tables in [26, 27]. Equation (4.1) and (4.2) are used in the calculation of CI of data in context predictor which is given by

$$CI = UCL - LCL \quad (4.3)$$

From the analysis made on ECG data collected from different patients, the features tend to follow log-normal distribution which is the case in most of the physiological signals. Every time the pre-processing block switches on, it collects the data for 8 seconds and the features corresponding to the data collected are fed to the context predictor. The context predictor calculates the confidence interval for mean of the features and compares it with threshold. If the threshold is not exceeded, it forces the pre-processing block into sleep state for some fixed duration. The sampling duration has to be chosen based on the wake up time of the sensors. The ECG sensors in general have a very less wake up time, which makes the 8 seconds sampling interval a reasonable selection. If in the first phase, the confidence interval has exceeded the threshold, the pre-processing block again samples for 4 seconds. Now the context predictor calculates the CI on the features extracted from the complete 12 seconds interval and based on the value of CI, it re-decides on the sampling.

Possible reasons behind the calculated CI exceeding beyond the threshold are improper electrode contacts, which generate incorrect features or the person might be suffering from myocardial infarction (heart attack), whose PR, QRS and QT intervals fluctuate rapidly for about 30 min. In such cases, if the convergence of the CI below the threshold is happening at a very long period, it can be considered as a myocardial infarction and the system triggers an alarm indicating for a proactive diagnosis. The complete flow of the context predictor is depicted in Fig. 4.3.

4.3 Performance analysis

For the performance analysis of the proposed architecture ECG data collected from 10 patients using the in house developed ECG data acquisition unit is used and the metrics used for the analysis are duty cycle, mean deviation, data rate generated and energy savings. The analysis makes use of 30

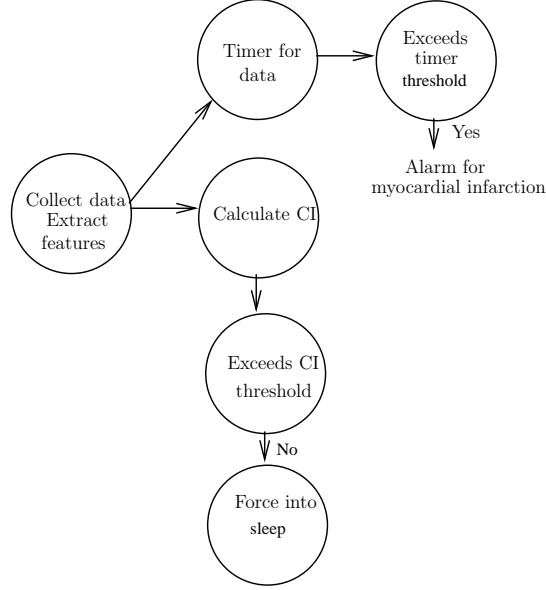


Figure 4.3: Flow of on-chip context predictor in different scenarios

seconds of ECG data collected from every patient due to the reason that in all the cases the CI has converged within 30 seconds. Fig. 4.4 shows the original ECG signal collected from the patient and the sampled signal obtained by using the proposed architecture. From the Fig. 4.4, one can observe the sleep time achieved by using the on-chip context predictor based intelligent sampling. On an average of 30 seconds over 10 patients, the duty cycle of the system is observed to be 27.99%. Fig. 4.5 shows the mean of PR interval extracted from the original signal of 30 seconds duration and sampled signal obtained by the proposed architecture from the original signal. The average deviation of features extracted from the sampled signal compared to the features extracted from the original signal, taken over all the 10 patients is observed to be 0.0032 seconds which is a negligible deviation. Hence the proposed architecture also provides the statistical guarantee.

The proposed architecture also aids for the reduction in the network traffic by reducing the amount of data generated. Fig. 4.6, shows the amount of data generated for all the 10 patients for period of 30 seconds when using the on-chip context predictor based intelligent sampling. On an average, there is a 72% of reduction in the amount of data generated, which is a significant reduction in IoT scenario.

Fig. 4.7, shows the energy saving obtained for each patient. The energy saving obtained for patient 2 is lesser when compared with other patients, due to the slower convergence of the confidence interval. An average of 72% energy saving over 10 patients for the sensing unit has been obtained by using the proposed intelligent sparse sensing architecture, which is a significant amount of saving.

4.4 Summary

In this chapter we proposed an on-chip context predictor based intelligent sparse sampling and smart transmission architecture for IoT enabled remote health monitoring applications. The proposed architecture greatly aids for achieving a significant reduction in the duty cycle of the system thereby

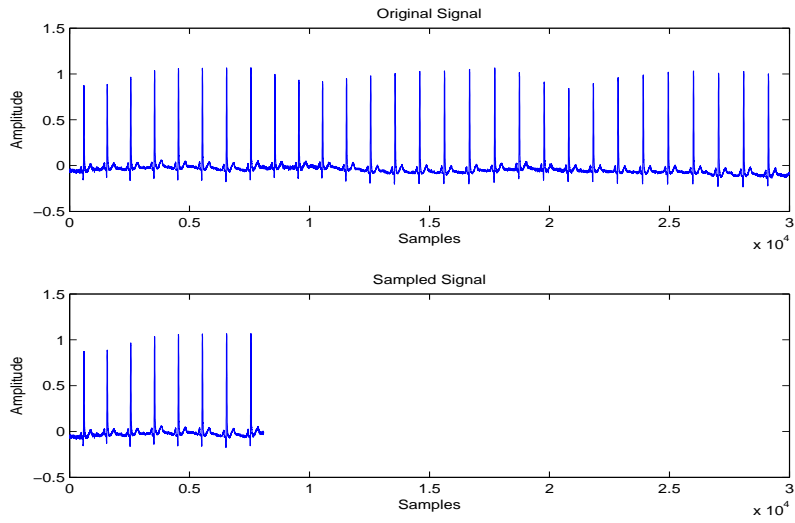


Figure 4.4: Original and sampled signals

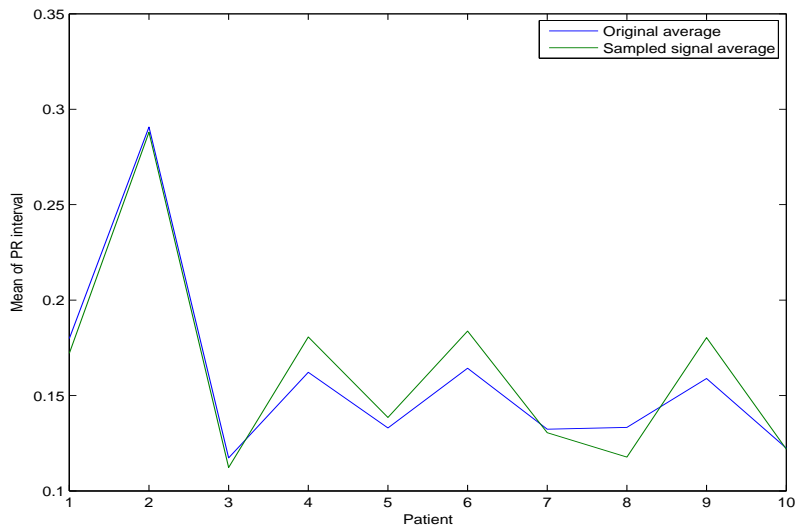


Figure 4.5: Mean of PR interval over 30 sec interval for original and sampled signals

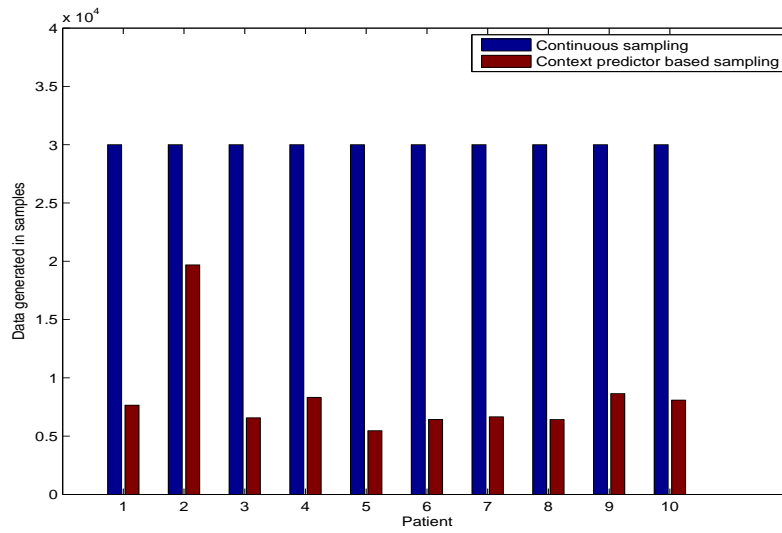


Figure 4.6: Amount of data generated

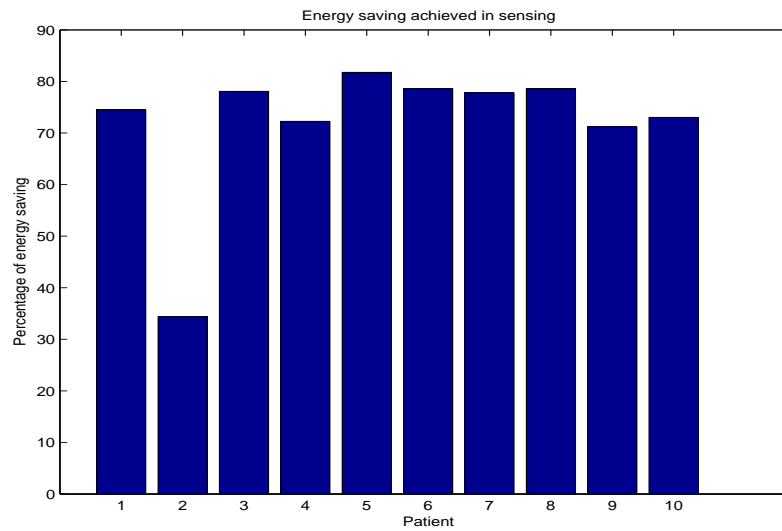


Figure 4.7: Energy saving obtained for each patient

reducing energy consumption and the amount of data rate generated while maintaining the statistical guarantee of the data collected. This architecture when analyzed on the ECG data collected using the in house developed ECG data acquisition system at IIT Hyderabad from 10 patients, achieved a duty cycle of 27.99% and 72% of reduction in data generated on an average taken over a 30 seconds interval. On an average over 10 patients, the proposed architecture achieved an energy saving of 72%, which is a significant amount of saving in remote health monitoring applications.

The analysis shown above is also performed using the ECG data from "The PTB Diagnostic ECG Database" [28, 29], which also yielded the similar performance.

Chapter 5

IEEE 802.15.4-PHY

Baseband processing in IEEE 802.15.4-PHY involves the modulation of the digital message signal along with performance enhancement techniques. The key performance enhancement techniques used in the IEEE 802.15.4-PHY are spreading and pulse shaping. ZigBee is one of the most successful applications of IEEE 802.15.4 std. It makes use of the MAC and PHY layer defined in the standard, and the upper layers (Application layer) are open to the users. The standard mainly concentrates on the low power devices, which can be used in general sensing or control applications, but not limited to. This makes ZigBee a widely used device in the field of Wireless Sensor Networks (WSNs) and Body Area Networks (BANs). The architecture for the IEEE 802.15.4-PHY is shown in the Fig. 5.1. The input data rate supported by the standard is 250 Kbps and message signal is modulated using a carrier frequency of 2.4 GHz. It uses O-QPSK as the modulation scheme, due to low hardware complexity than QPSK. The architecture uses DSSS which maps four bit message symbols to a predefined 32 bit chip sequences [1]. Traditional architecture makes use of Half-Sine pulse shaping with Offset QPSK resulting to Minimum Shift Keying (MSK) for modulation. In this section the performance of DSSS with O-QPSK modulation is evaluated and then the performance of DSSS in the presence of pulse shaping is presented.

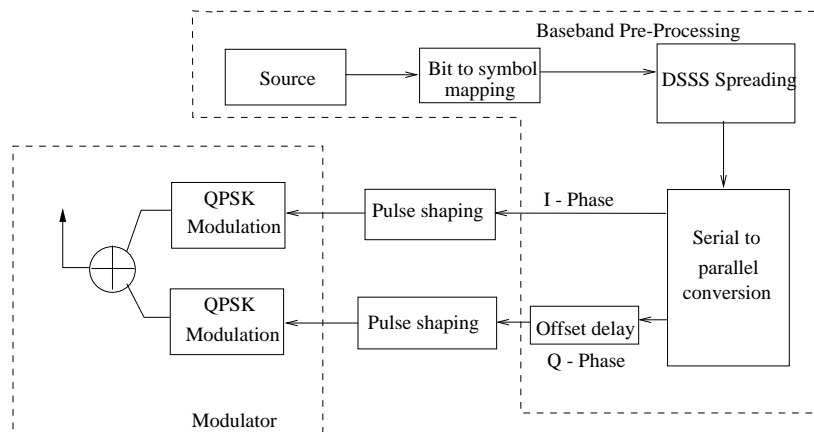


Figure 5.1: Architecture of IEEE 802.15.4-PHY transmitter

Symbol	Chip sequence
0000	11011001110000110101001000101110
1000	11101101100111000011010100100010
0100	00101110110110011100001101010010
1100	00100010111011011001110000110101
0010	01010010001011101101100111000011
1010	00110101001000101110110110011100
0110	11000011010100100010111011011001
1110	10011100001101010010001011101101
0001	10001100100101100000011101111011
1001	10111000110010010110000001110111
0101	01111011100011001001011000000111
1101	01110111101110001100100101100000
0011	00000111011110111000110010010110
1011	01100000011101111011100011001001
0111	10010110000001110111101110001100
1111	11001001011000000111011110111000

Table 5.1: Symbol to chip mapping

5.1 Performance evaluation of IEEE 802.15.4-PHY without pulse shaping (only DSSS)

DSSS in IEEE 802.15.4-PHY maps four bit message symbols to 32 bit chip sequences. The predefined chip sequences are shown in Table 5.1. Upon mapping, the information signal is spread over a large bandwidth. Selection of chip sequences uses the minimum similarity criteria which is measured using the cross correlation. The chip sequences used here are quasi orthogonal (not perfectly orthogonal).

Fig. 5.2 plots the BER versus different symbol energies for O-QPSK system with and without DSSS. We can see the significant improvement in BER when using DSSS. This is due to the anti jam characteristics offered by spreading techniques. When DSSS is used, the receiver reconstructs the desired signal and at the same time the interference signal energy is spread across a wide bandwidth [45], which increases the SNR at receiver in required band of frequencies, thereby providing anti jam characteristics.

5.2 Performance evaluation of IEEE 802.15.4-PHY (with DSSS and pulse shaping)

In [46], the authors evaluated the performance of MSK in the presence of Frequency Hop Spread Spectrum and performance of MSK and in [47], the performance of MSK with DSSS generated using PN sequence generators are evaluated. In this section we evaluated the performance of MSK in the presence of DSSS using the IEEE PN sequences as defined by IEEE 802.15.4-PHY standard. Fig. 5.3 compares the BER performance versus various SNRs for O-QPSK, MSK and IEEE 802.15.4-PHY (MSK + DSSS). The MSK receiver here uses one bit duration (T_b) for decoding the received signal, resulting in the degradation of MSK performance compared to O-QPSK. From Fig. 5.3, one can clearly observe the degradation in BER performance when MSK is combined with DSSS. The

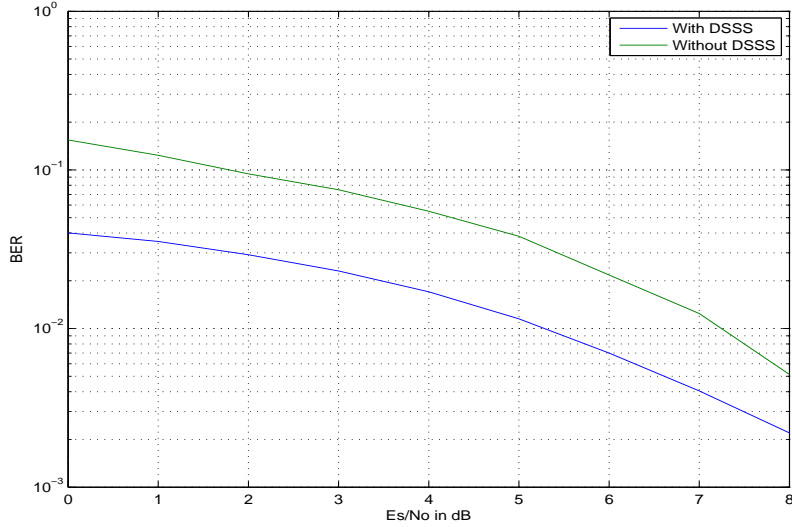


Figure 5.2: BER curves for O-QPSK with and without DSSS

advantage of MSK modulated DSSS spread signal than O-QPSK modulated DSSS spread signal is the battery power efficiency [48] which is an important aspect of ZigBee. Digital modulation methods with constant envelope signals are more battery efficient than those with modulated envelope signals since the latter require inefficient linear radio frequency amplifiers. Usage of MSK also results in a constant envelope with continuous phase. The mathematical formulation of MSK is shown in equation (5.1).

$$s(t) = \sqrt{\frac{2E_b}{T_b}} \cos(2\pi f_c t + \theta(t)) \quad (5.1)$$

In equation (5.1), $s(t)$, E_b , T_b represents MSK modulated signal, signal energy per bit and bit duration respectively. f_c and $\theta(t)$ represents carrier frequency and phase of the modulated signal. In the signal bandwidth perspective, the side lobes are better suppressed in MSK than O-QPSK, resulting in less co-channel interference. Fig. 5.4 and Fig. 5.5 shows the frequency spectrum of signals modulated using MSK and O-QPSK respectively. The signal modulated using MSK has a larger major lobe than O-QPSK modulated signal. Whereas in MSK, the side lobes are quickly and better suppressed compared to O-QPSK modulated signal. The carrier frequency used for analysis is 2.5 MHz.

5.3 Different Pulse Shaping Techniques

IEEE 802.11b uses the Raised Cosine pulse shaping technique along with CCK spreading. For targeting multiple radios in remote deployment applications especially in remote health monitoring applications, the form factor is a major constrain. Hence reusing the design is one of the primary approaches in reducing the area consumption. In order to exploit the design reuse the commonly available functional units in different architectures have to be multiplexed. Hence in this section we evaluate the performance of three different widely used pulse shaping techniques. We compare

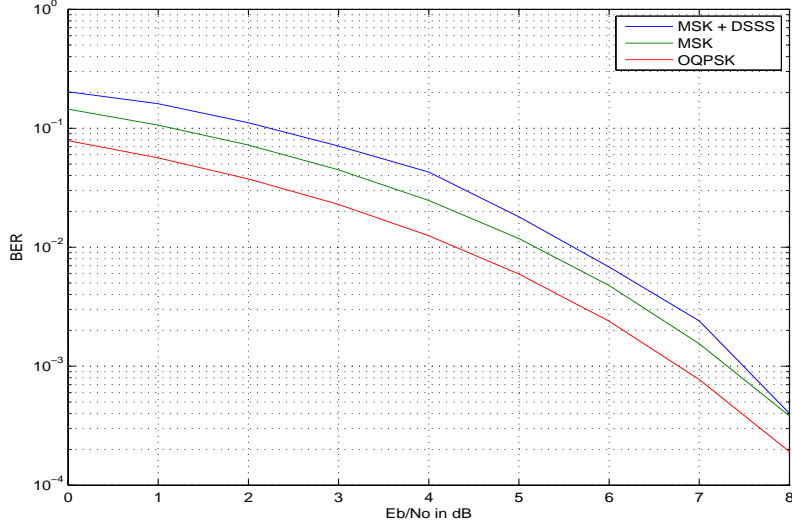


Figure 5.3: BER curves for IEEE 802.15.4-PHY compared to MSK

the BER performance of three different pulse shaping techniques namely Raised Cosine (RC), Root Raised Cosine (RRC) and Half Sine (HS) pulse shaping with O-QPSK modulation. The architecture for performance analysis of different pulse shaping techniques is shown in Fig. 5.6. The impulse response of all the three pulse shaping techniques are given in equations (5.2, 5.3 & 5.5)

1) Half sine pulse shaping: The impulse response used for pulse shaping is a half sine as shown in Fig. 5.7, which can be characterized by equation (5.2) [49].

$$h(t) = \sin\left(\frac{\pi t}{2T_b}\right), \quad 0 \leq t \leq 2T_b \quad (5.2)$$

Here T_b indicates the bit duration and $h(t)$ is the time domain impulse response.

2) Raised cosine pulse shaping: It is one of the most widely used techniques for pulse shaping. It minimizes the ISI by attenuating the symbol boundaries, because these portions play prominent role in creating the ISI issues. The impulse response can be characterized as shown in (5.3) [50]. Fig. 5.8 plots the impulse response of raised cosine pulse shaping transmit filter.

$$h(t) = \text{sinc}(2\omega t) \left(\frac{\cos(2\pi\alpha\omega t)}{1 - 16\alpha^2\omega^2 t^2} \right) \quad (5.3)$$

$$\omega = \frac{2\pi}{T_b} \quad (5.4)$$

In equation (5.3), $h(t)$ is the time domain impulse response. α and T_b refers to roll of factor and bit duration respectively. The value of α considered for the performance analysis is 0.25

3) Root raised cosine pulse shaping: The frequency response of transmit filter for root raised cosine is square root of the frequency response of raised cosine filter [51]. The impulse response is shown

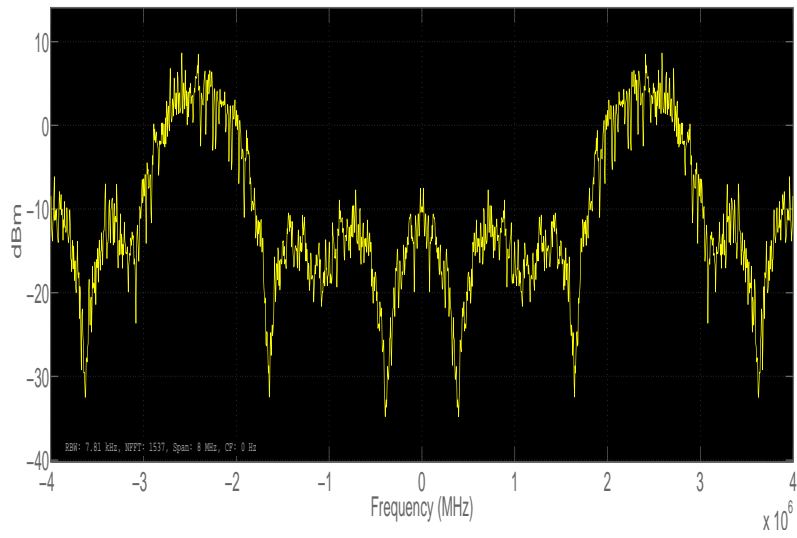


Figure 5.4: Frequency spectrum of MSK modulated signal

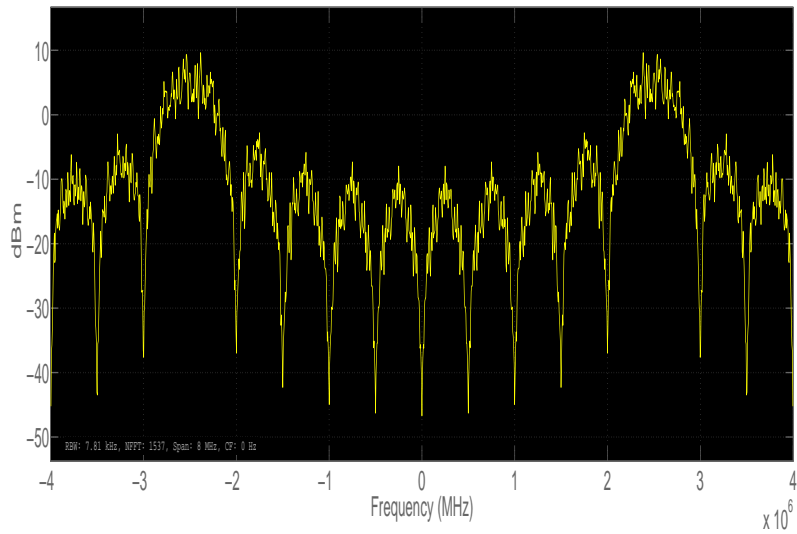


Figure 5.5: Frequency spectrum of QPSK modulated signal

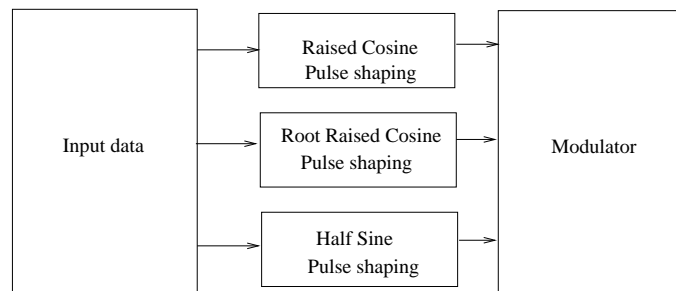


Figure 5.6: IEEE 802.15.4-PHY Architecture with different pulse shaping techniques

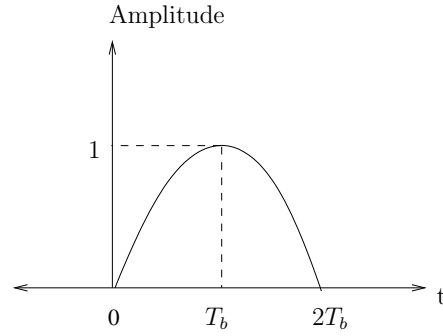


Figure 5.7: Impulse response of half sine pulse shaping filter

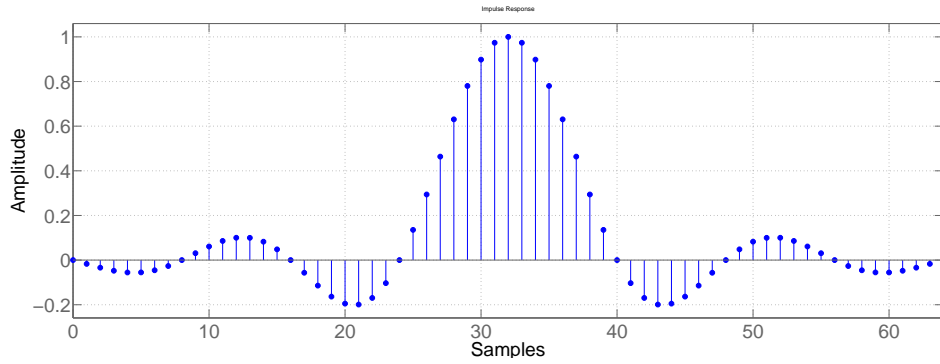


Figure 5.8: Impulse response of raised cosine pulse shaping filter

in Fig. 5.9 and is characterized by equation (5.5).

$$h(t) = \begin{cases} \frac{1}{\sqrt{T_b}} \left(1 - \alpha + \frac{4\alpha}{\pi}\right), & t = 0 \\ \frac{\alpha}{\sqrt{2T_b}} \left[\left(1 + \frac{2}{\pi}\right) \sin\left(\frac{\pi}{4\alpha}\right) + \left(1 - \frac{2}{\pi}\right) \cos\left(\frac{\pi}{4\alpha}\right) \right], & t = \pm \frac{T_b}{4\alpha} \\ \frac{1}{\sqrt{T_b}} \frac{\sin\left(\frac{\pi t(1-\alpha)}{T_b}\right) + \frac{4\alpha t}{T_b} \cos\left(\frac{\pi t(1+\alpha)}{T_b}\right)}{\frac{\pi t}{T_b} \left(1 - \left(\frac{4\alpha t}{T_b}\right)^2\right)}, & \text{otherwise} \end{cases} \quad (5.5)$$

Here T_b , α and $h(t)$ indicates the bit duration, roll off factor and time domain impulse response

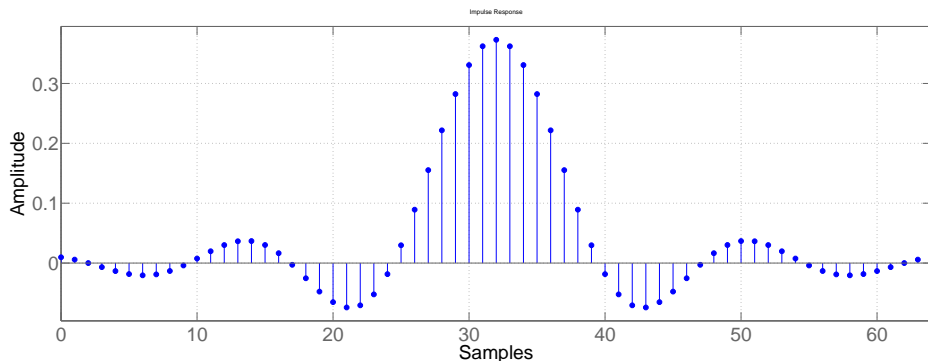


Figure 5.9: Impulse response of root-raised cosine pulse shaping filter

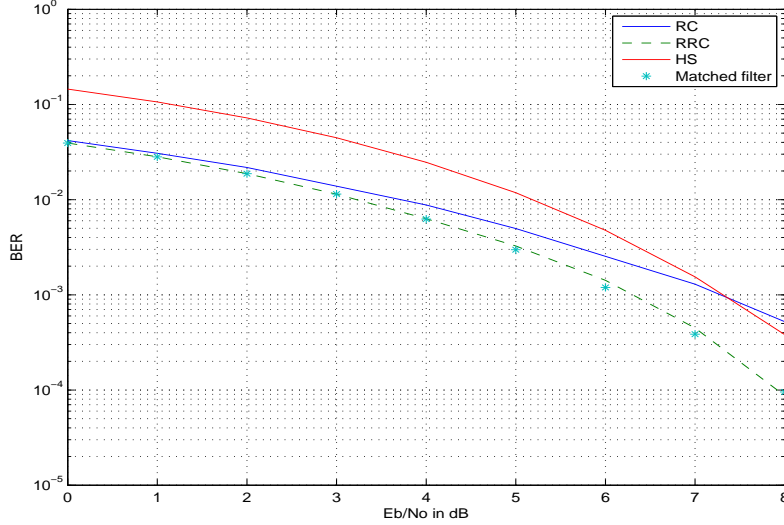


Figure 5.10: Comparison of noise performances for RC, RRC and HS pulse shaping techniques

respectively. The value of α considered for the performance analysis is 0.25.

5.4 Performance analysis of different pulse shaping techniques

In this work, we intend to compare the noise performance of all three pulse shaping techniques. Fig. 5.10 plots the BER versus SNR of all the three pulse shaping techniques namely RC, RRC and HS pulse shaping. For the performance analysis spreading is not taken into account. From Fig. 5.10, RRC pulse shaping delivers better performance than rest of the two pulse shaping techniques under Additive White Gaussian Noise (AWGN) channel conditions. When using RRC pulse shaping the receiver uses matched filter for decoding the received pulse shaped sequences. The matched filter is the optimal linear filter for maximizing the signal to noise ratio (SNR) in the presence of additive stochastic noise. The impulse response of the root-raised cosine receive filter is same as that of root-raised cosine transmit filter. The approximate BER achieved by using the matched filter in terms of signal energy per bit is given by (5.6).

$$P_e \approx \frac{1}{4} \operatorname{erfc} \left(\sqrt{\frac{E_b}{N_o}} \right) \quad (5.6)$$

In equation (5.6), E_b refers to signal energy per bit and $\frac{N_o}{2}$ is the noise power spectral density. The BER performance of root-raised cosine and matched filter are shown in Fig. 5.10. From Fig. 5.10, the performance of half sine pulse shaping is noticeably degraded at low SNRs when compared with raised cosine and root raised cosine techniques, due to the less attenuation provided in out of band frequencies than raised cosine and root raised cosine pulse shaping. However at high SNRs, the performance of half sine pulse shaping dominates performance of raised cosine pulse shaping.

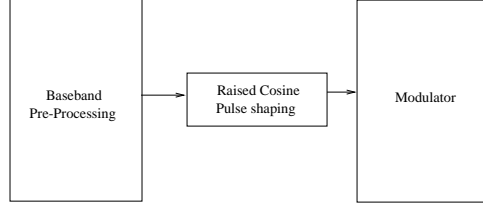


Figure 5.11: Architecture of proposed modified IEEE 802.15.4-PHY transmitter

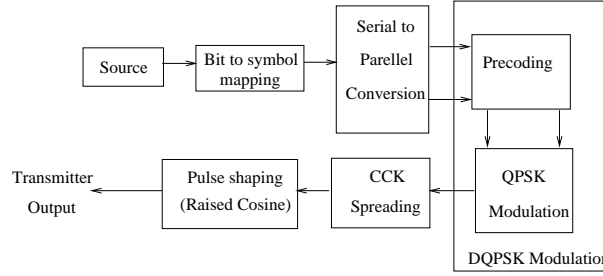


Figure 5.12: Architecture of IEEE 802.11b transmitter

5.5 Performance Evaluation of Proposed Modified IEEE 802.15.4-PHY

The usage of multiple radio gateways can greatly aid for ubiquitous connectivity and support large number of applications. IEEE P1905.1 standard [40] defines an abstraction layer which provides common interface to widely deployed home networking technologies. We propose a modified IEEE 802.15.4 architecture which uses raised cosine pulse shaping technique. The modified IEEE 802.15.4-PHY architecture is shown in Fig. 5.11 enables the multiplexing of pulse shaping functional unit in both the IEEE 802.15.4 and IEEE 802.11b standards. Fig. 5.12 show the transmitter architecture for IEEE 802.11b. The BER performances of the proposed modified IEEE 802.15.4-PHY and IEEE 802.15.4-PHY are analyzed and shown in Fig. 5.13. It is observed that, the performance of raised cosine and half sine pulse shaping along with DSSS is similar at low values of SNR, but gradually half sine pulse shaping dominates the performance of raised cosine at high values of SNR. The advantages of using Raised Cosine pulse shaping is the ease of digital FIR implementation and architecture multiplex when using multiple radios. IEEE 802.11b uses raised cosine pulse shaping technique, which is a well established standard and is more suitable for long range Personal Area Networks (PANs). The other advantages of using modified IEEE 802.15.4-PHY architecture is the ease of adaptability since the IEEE 802.11b standard is widely established and easily available. Upon using the modified IEEE 802.15.4-PHY, the area reduction achieved in the multiplexed architecture of IEEE 802.15.4 and IEEE 802.11b can be significant.

5.6 Summary

In this paper, we analyzed the noise performance of IEEE 802.15.4-PHY along with three different pulse shaping techniques namely Raised Cosine, Root-Raised Cosine, Half-Sine pulse shaping. The

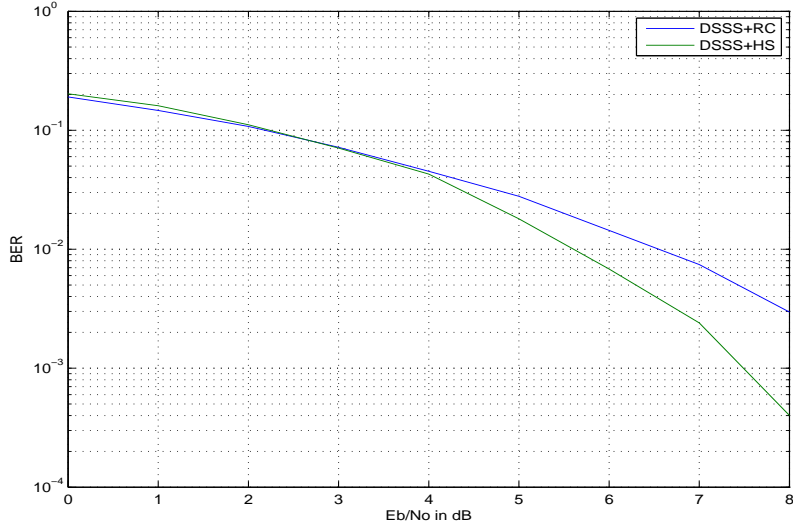


Figure 5.13: Comparison of BER performances for proposed modified IEEE 802.15.4-PHY and traditional IEEE 802.15.4-PHY

analysis shows that the performance of root-raised cosine pulse shaping dominates the rest of the two pulse shaping techniques. Upon combining the pulse shaping with IEEE 802.15.4 standard specified DSSS, the performance is degraded than O-QPSK system without spreading and pulse shaping. We also discussed a modied IEEE 802.15.4-PHY, which uses Raised Cosine pulse shaping and whose performance is similar to IEEE 802.15.4-PHY with Half Sine pulse shaping at low SNRs. The modified IEEE 802.15.4-PHY when used along with IEEE 802.11b can significantly aid for design reuse of pulse shaping filter, thereby achieving multiplexed architecture and area optimization in on-chip multiple radios.

Our future scope is to multiplex and optimize the architectures of IEEE 802.15.4 and IEEE 802.11b for minimum area implementation with maximum energy saving and develop an on-chip architecture multiplexed IoT enabled multiple radio gateway.

Chapter 6

Architecture of the mixer less QPSK modulator system

Fig. 6.1 shows the traditional transmitter architecture which most of the architectures employ. It generally consists of a LO stage which generates the carrier signal and mixer which up-converts the base band signal to pass band. In this section we discuss the architecture of the complete low complex QPSK based transmitter system which is shown in Fig. 6.2. In the following subsections each of the functional units involved in the proposed low complex architecture has been described briefly.

6.1 QPSK modulation

Digital modulation bridges the transmission of digital symbol into wireless medium [35, 34, 36]. A sequence of digital symbols are used to alter the characteristics of the carrier. The bandwidth and bit rate depends on the modulation scheme we use. In QPSK we use two quadrature carriers (sine and cosine). Each of the message symbol is divided into two phases, in phase and quadrature phase components which uses the two carriers for modulation. The number of bits transmitted in each of

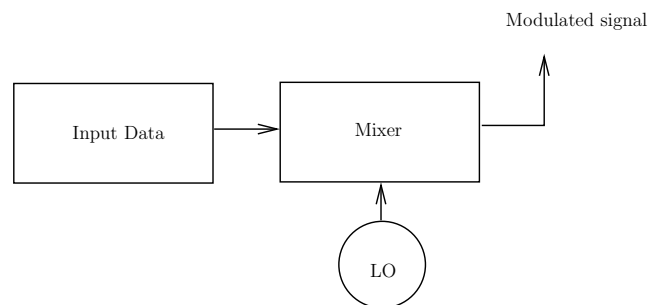


Figure 6.1: Proposed architecture of low complex QPSK modulator

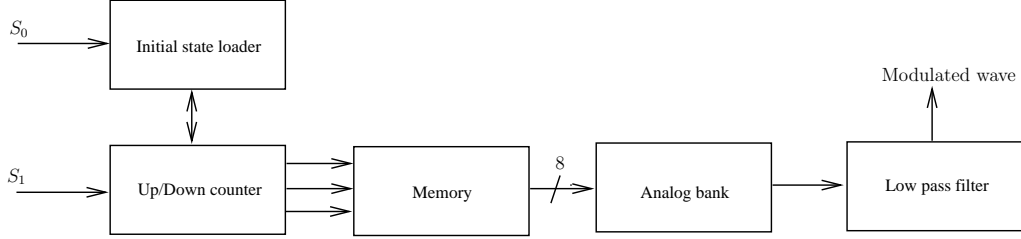


Figure 6.2: Proposed architecture of low complex QPSK modulator

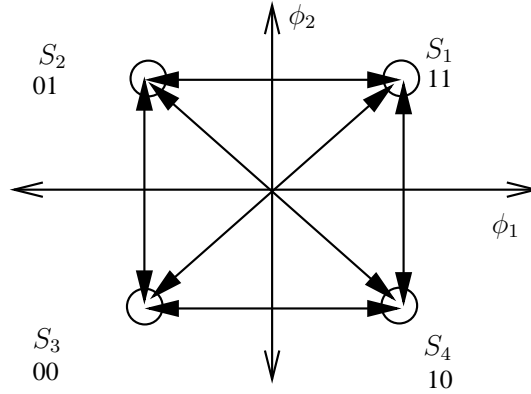


Figure 6.3: Constellation diagram for QPSK system

the phases are same. The mathematical definition of the QPSK signal can be stated as shown below

$$S_i(t) = \begin{cases} \sqrt{\frac{2E}{T}} \cos(2\pi f_c t + \theta_i), & 0 \leq t \leq T \\ 0, & \textit{otherwise} \end{cases} \quad (6.1)$$

$$\theta_i = (2i - 1) \frac{\pi}{4} \quad (6.2)$$

In (6.1), $S_i(t)$ indicates the modulated wave, f_c represents the carrier frequency or center frequency and i varies from 1 to 4 indicating the message symbol. θ_i denotes the phase associated with the i^{th} message symbol, T is the symbol duration and E is the transmitted signal energy per symbol. Upon expanding (1), it results in the following form

$$S_i(t) = \sqrt{\frac{2E}{T}} \cos \left[(2i - 1) \frac{\pi}{4} \right] \cos(2\pi f_c t) - \sqrt{\frac{2E}{T}} \sin \left[(2i - 1) \frac{\pi}{4} \right] \sin(2\pi f_c t) \quad (6.3)$$

The constellation diagram can be realized as shown in Fig. 6.3 and the signal space characterization is shown in Table 6.1. In Fig. 6.3, all possible phase transitions have been indicated with the arrows. The maximum phase shift possible is 180° which are indicated by the diagonal arrows. All the possible input message symbols are represented with S_1 , S_2 , S_3 and S_4 in the constellation diagram. For a detailed description on the QPSK system, one can refer to [35] & [37].

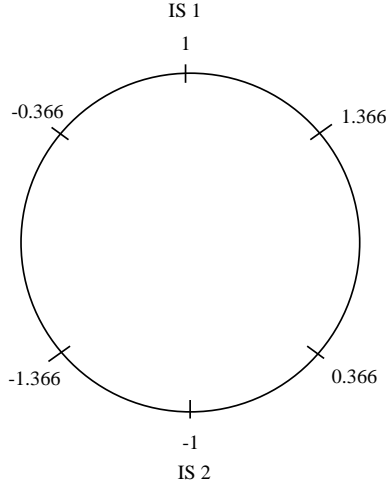


Figure 6.4: Symbol cycle of a QPSK system

Input symbol	Phase of QPSK signal	Coordinates on constellation diagram
10	$\frac{7\pi}{4}$	$(\sqrt{\frac{E}{2}}, -\sqrt{\frac{E}{2}})$
00	$\frac{5\pi}{4}$	$(-\sqrt{\frac{E}{2}}, -\sqrt{\frac{E}{2}})$
01	$\frac{3\pi}{4}$	$(-\sqrt{\frac{E}{2}}, \sqrt{\frac{E}{2}})$
11	$\frac{\pi}{4}$	$(\sqrt{\frac{E}{2}}, \sqrt{\frac{E}{2}})$

Table 6.1: Signal space characterization for QPSK system

We assume the carrier frequency to be f_c . Upon using a sampling rate of $6f_c$, symbol energy of T in a single period of modulated signal we can have six discrete samples of the modulated signal. Considering the first case where the message symbol is 10, the sampled signal and the discrete sample values of the modulated signal can be represented as below.

$$\begin{aligned}
 S(n) &= \cos(2\pi f_c n T_s) - \sin(2\pi f_c n T_s) \\
 S(0) &= 1, S(1) = -0.366, S(2) = -1.366, \\
 S(3) &= -1, S(4) = 0.366, S(5) = 1.366
 \end{aligned} \tag{6.4}$$

Now sampling the modulated wave for all four message symbols, each of them results into the following samples as shown in Table 6.2 in a single period of the modulated signal.

6.2 Symbol cycle

In Table 6.2, all the six samples are same for all the 4 message symbols. The only difference is in the occurrence of those samples in the time series. The message symbols 11 and 10 has the same first sample '1' and the rest of the samples are reverse in order for message symbol 10 compared with the message symbol 11. The symbol cycle for the QPSK system for a symbol energy of T is

Input symbol	Modulated signal	Set of samples
11	$S_1(t) = \cos(2\pi f_c t) - \sin(2\pi f_c t)$	{ 1, 1.366, 0.366, -1, -1.366, -0.366 }
10	$S_2(t) = -\cos(2\pi f_c t) - \sin(2\pi f_c t)$	{1, -0.366, -1.366, -1, 0.366, 1.366 }
01	$S_3(t) = -\cos(2\pi f_c t) + \sin(2\pi f_c t)$	{-1, 0.366, 1.366, 1, -0.366, -1.366 }
00	$S_4(t) = \cos(2\pi f_c t) + \sin(2\pi f_c t)$	{-1, -1.366, -0.366, 1, 1.366, 0.366 }

Table 6.2: Samples of modulated signal corresponding to individual message symbol

Input symbol	Initial state
11 & 10	IS1
01 & 00	IS2

Table 6.3: Initial states corresponding to individual message symbol

shown in Fig. 6.4. In the symbol cycle IS-1 denotes the initial state 1 and IS-2 denotes initial state 2. Initial state can be defined as the first discrete sample when the input message symbol changes. Whenever a new message symbol from the available symbols comes as an input, the first sample of the modulated signal is one of these two initial states. The choice of initial states are shown in Table 6.3.

The initial state depends only on the I phase component of the message symbol and the following samples in the modulated signal depends on the Q phase component of the message symbol. If the Q phase component of the message symbol is 0, the symbol cycle is traversed in anticlockwise direction else the symbol cycle is traversed clockwise with reference to the initial state. The same set of six samples are periodically repeated for the entire symbol duration which results in the discrete QPSK modulated wave as shown in Fig. 6.5. For modulating a digital symbol now the process can be of generating these samples at a periodic intervals continuously after deciding the initial state and the symbol cycle traversal.

6.3 Analog bank

The analog bank generates all the six individual samples based on an eight bit keying sequence as input. It is developed using BJTs, which aids in a low complex design and low cost. The in house developed analog bank at IIT Hyderabad is shown in Fig 6.6. The main aim in developing using the BJTs is their ease of fabrication and the low power consumption. From the technology point of view the fabrication process of BJTs is well studied and established. Other advantage of the analog bank is to reduce the complexity of integration in the mixed signal design (digital base band and RF). The analog bank operates in co-joint with the counter controlled memory unit which operates using LVCMOS33 standard. All the transistors used in the construction of prototype for the analog bank are operated in the common emitter configuration and requires 3.3 V dual power supply. The prototype for analog bank is constructed with the 2N2222A NPN transistors [38], 2N3702 PNP transistors [39] and resistors. It does not consists of any storage elements which makes the fabrication much easier and low area.

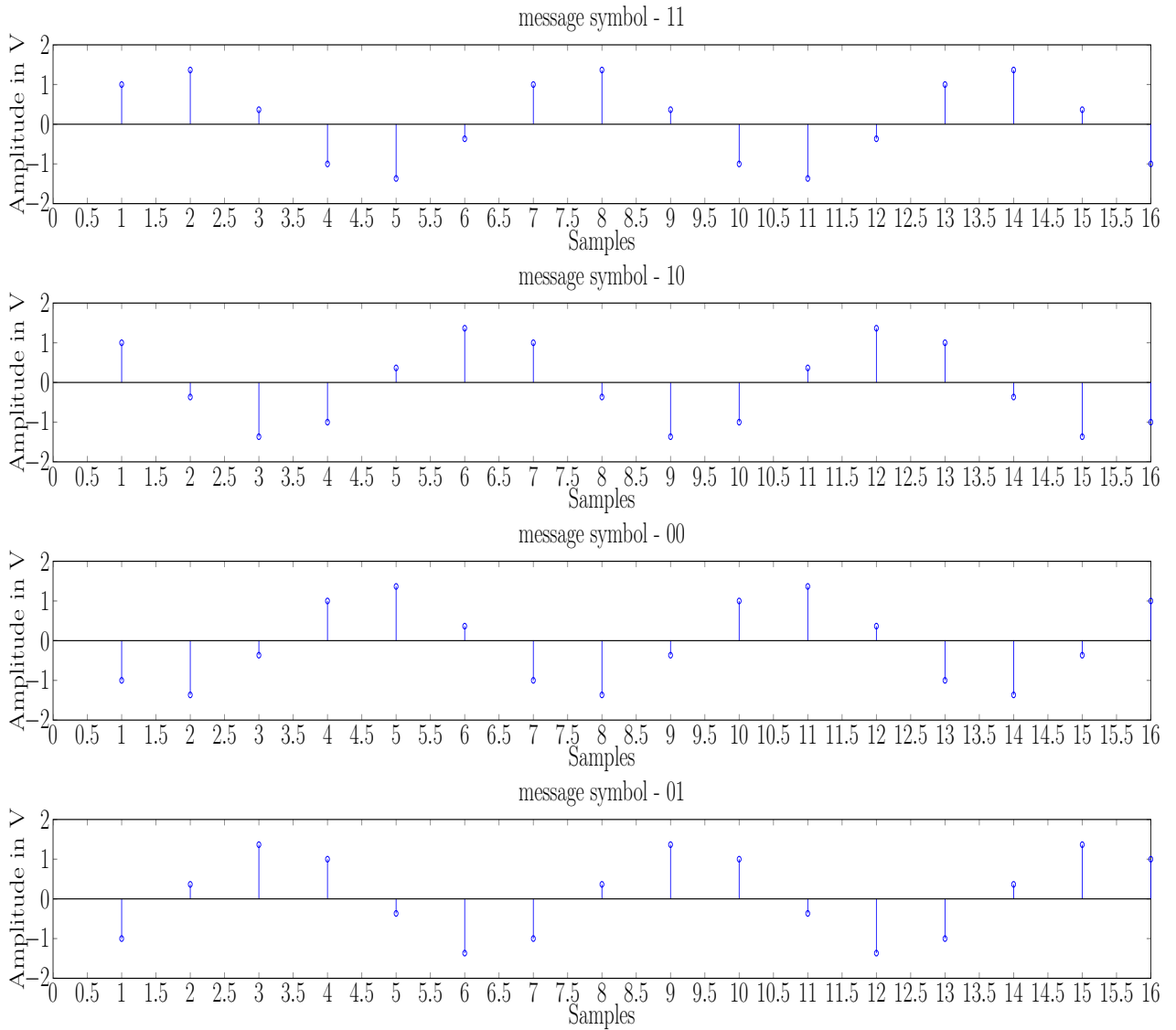


Figure 6.5: Sampled signal of the QPSK modulated wave for 4 symbols

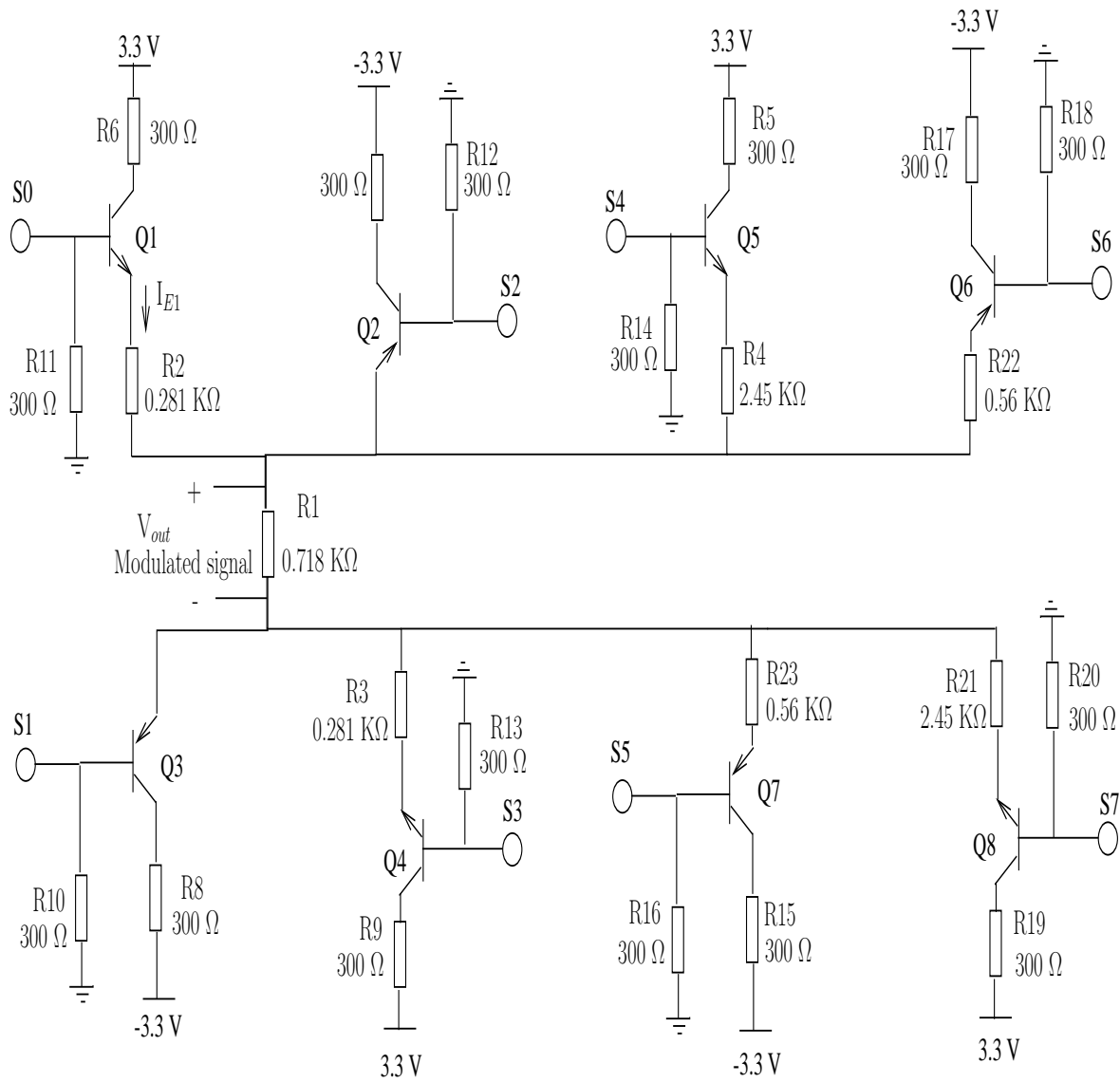


Figure 6.6: Proposed architecture of analog bank

Address location	Input keying sequence S[0:7]	Output amplitude
000	10100110	1.36602
001	01101010	0.36602
010	01010010	-1
011	01010110	-1.36602
100	01100101	-0.36602
101	10100100	1

Table 6.4: Address location for the keying sequence and corresponding output sample produced by analog bank

The keying sequence provided at the 8 bit input of the analog bank decides the output voltage across the resistor R_1 . The output voltages for the corresponding input keying sequence are shown in Table 6.4. If the keying sequence provided by the memory unit is 10100110, voltages at S0, S2, S5 and S6 are 3.3 V whereas at S1, S3, S4, S7 are 0 V. The transistors Q2, Q4, Q5, Q6, Q7 and Q8 will be in cut-off region. Transistors Q1 and Q3 will be in active region. The current passing through the resistor R1 is then equal to I_{E1} . Value of I_{E1} can be calculated as shown below.

$$\begin{aligned}
 V_{S0} &= 3.3 \text{ V}, V_{BE1} = 0.7 \text{ V}, V_{BE2} = 0.7 \text{ V} \\
 I_{E1} &= \frac{V_{S0} - V_{BE1} - V_{BE2}}{0.281K + 0.718K} = 1.90mA \\
 V_{out} &= I_{E1}R_1 = 1.36V
 \end{aligned} \tag{6.5}$$

Upon providing a proper keying sequence, we can generate the necessary amplitudes. Using the analog bank we can now generate the samples for the modulated wave. For providing the keying sequence for the analog bank we use the memory which is controlled by a counter and initial state loader.

6.4 Memory

Memory generates the keying sequence for analog bank depending on the input fed by the counter. The keying sequences for all the six samples are stored in successive memory locations. Based on the input address provided to the memory functional unit, proper output sequence can be generated. The output sequence generated then triggers the analog bank to generate the required output sample. The memory used is of 8 bit width and 6 bytes depth. Table 6.4 shows the address location of the memory storage and the corresponding data stored in the address. LVCMOS33 standard is used for the memory output, logic level 1 is represented with 3.3 V and logic level 0 is represented with 0 V. The transition width during switching should be made as small as possible to achieve better accuracy for the modulated wave.

6.5 Up/Down counter

It is used for selecting the appropriate memory location which can generate the required samples at the output from analog bank. The functionality of the up/down counter is to count the values in the range of 0 to 5 in up or down fashion. The selection of up or down counting depends on the Q phase component of the message symbol. If the Q phase component is 0 the counting is in down fashion

else it is in up fashion with reference to the initial state of the counter. The main aim of the counter is to organize the output samples according to the input message symbol. If the input message symbol is 11 the symbol cycle is traversed in clock wise direction. When the Q phase component is 1 the counter is up fashion and generates the analog samples from analog bank which implicates the symbol cycle being traversed in the clockwise direction. The initial state of the counter is loaded using the initial state loader. The clock frequency for the counter is the sampling rate we use, which depends on the center frequency we are targeting for the application. If we change the input clock frequency for the counter, the center frequency changes. The calculation of center frequency is given below

$$\begin{aligned}
 \text{Sampling frequency} &= f_s \\
 \text{Center frequency} &= f_c \\
 f_c &= \frac{f_s}{6}
 \end{aligned} \tag{6.6}$$

In the above equation, f_s is the sampling frequency and it is assumed to be six times the center frequency f_c . If we change the sampling frequency the center frequency of the modulated wave changes. Here the sampling frequency is determined by the clock frequency with which the counter operates. Targeting to a center frequency of 120 MHz will require a clock speed of 720 MHz for the counter.

6.6 Initial state loader

The initial state loader aids to reset the counter to an initial state every time the message symbol changes. If the message symbol is 11 the first sample in the modulated wave is 1.33 V, which can be generated by feeding the keying sequence stored in the memory location 000. When the message symbol changes to 11 at the input of the transmitter section, the counter should point to the memory location 000. The initial state loader points only to two states, IS-1 and IS-2. The keying sequences required to generate IS-1 and IS-2 are stored in memory locations 000 and 011. The initial state loader will only initialize the counter with any of these two values. The input to the initial state loader is the I phase component of the message symbol. If the I phase component is 1, the counter is initialized with the value 000 else it is initialized with 011.

6.7 Low pass filter

The low pass filter is a simple RC filter which eliminates the noises at high frequencies. It's primary use is to remove stair cases generated from the signal acquired from analog bank and generate a smooth continuous modulated signal, thereby eliminating co-channel interferences.

6.8 Performance analysis

A hardware prototype shown in Fig. 6.7 for the proposed architecture described above is developed in IIT Hyderabad. The center frequency targeted is 208.3 KHz, which requires a sampling rate of 1.25 MHz. The frequency supplied to the counter is 1.25 MHz. Architecture of the hardware

prototype is shown in Fig. 6.8. All the digital functional units have been implemented using Spartan 3E FPGA and the analog bank is developed in IIT Hyderabad. Fig. 6.10 shows the modulated signal acquired from the analog bank of the developed hardware prototype. From Fig. 6.10 one can infer the distortion in the signal at the hold positions, which are mainly caused due to the presence of the distortion in the keying sequence generated from the memory unit and can be eliminated upon using a low pass filter. The modulated signal generated after smoothening using a low pass filter is shown in Fig. 6.9. The analog bank is level sensitive to the keying sequence generated by the memory unit on the FPGA. The logic level high generated by the memory unit should have to maintain a voltage level of 3.3 V without any distortion. A better signal with higher frequency can be generated upon generating a good quality keying sequence from the FPGA, which is a limitation in the Spartan 3E FPGA. The prototype developed is observed to be a low complex due to the elimination of mixers. Due to rapid growing number of devices which may lead to hyper connectivity scenario, these low complex communication devices with less maintenance can aid for easy deployment in IoT and M2M applications. The prototype has been tested by generating various frequencies ranging from 1 KHz to 120 MHz, which resulted in similar performance as discussed above.

6.9 Summary

In this chapter we proposed a low complex mixer less QPSK based transmitter architecture using BJTs as primary elements in the analog bank which can greatly aid for IoT and M2M applications where the less design complexity is an important aspect. The architecture can also be developed using the MOSFET technology, with minor changes in the functional units of the architecture. A hardware prototype for the architecture proposed is developed in IIT Hyderabad and the generated modulated signal at a center frequency of 205.8 KHz has been analyzed. The quality of the modulated signal mainly depends on the quality of the signal generated by the memory unit. Lesser the distortion at the output of the memory unit, greater the quality of the modulated signal. The prototype developed is of low complex due to the elimination of mixers in the design. The other advantages of the proposed architecture are the ease of integration between digital functional units and the simple analog bank. The prototype developed at IIT Hyderabad has been successfully tested for generation of various frequencies ranging from 1 KHz to 120 MHz. With the enhancement of technology, even higher frequencies upto GHz range can be generated.

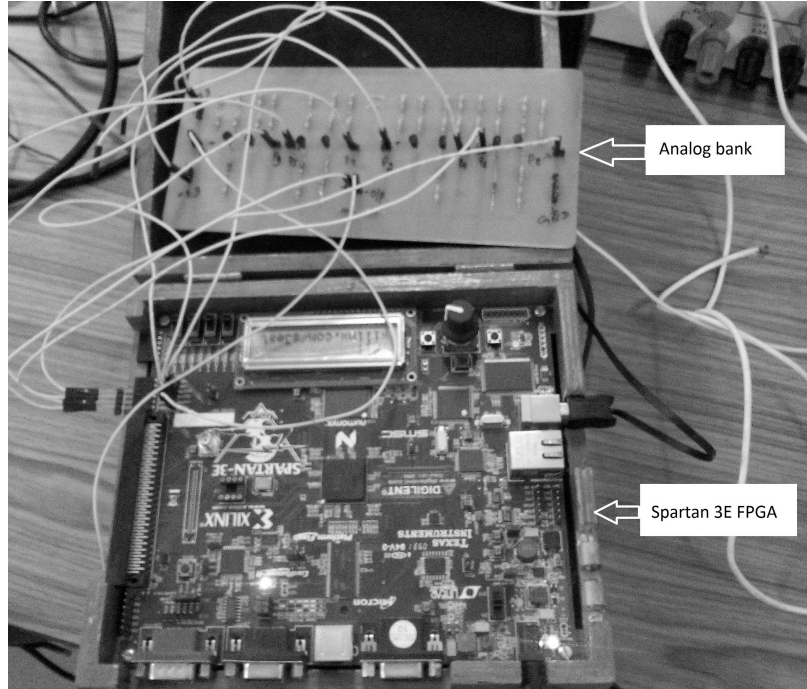


Figure 6.7: Hardware prototype of the proposed low complex QPSK based transmitter architecture developed in IIT Hyderabad

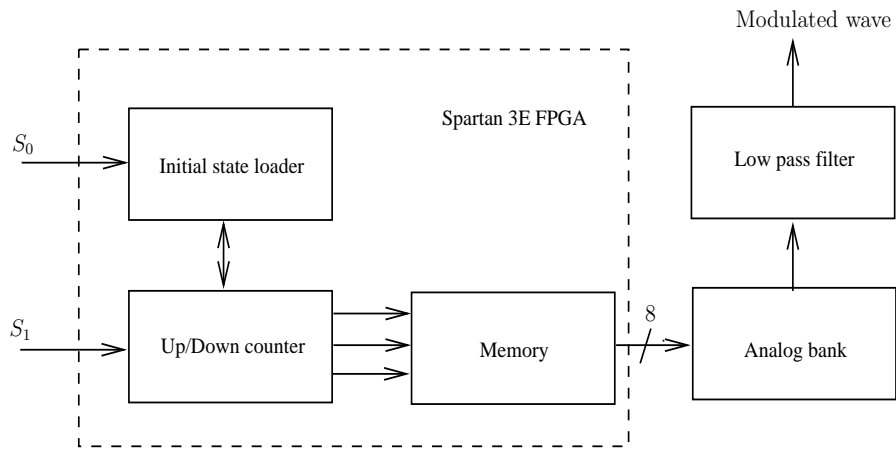


Figure 6.8: Architecture of the hardware prototype

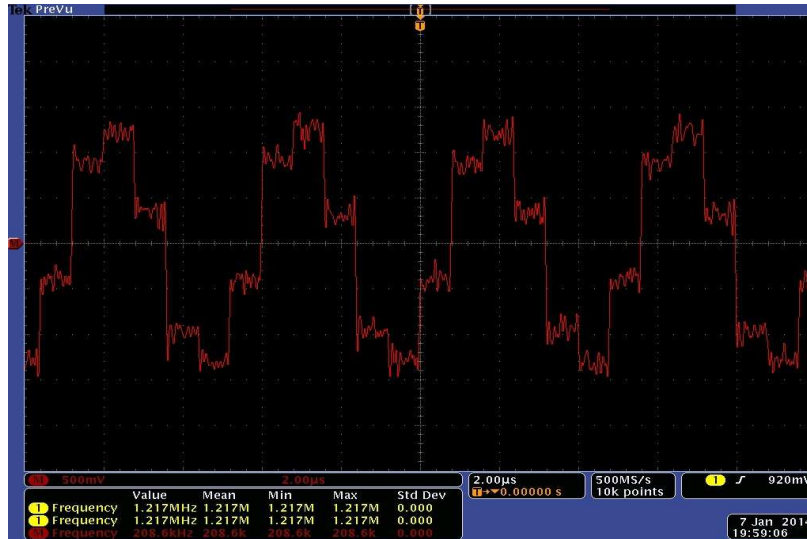


Figure 6.9: Modulated signal acquired from the analog bank of the developed hardware prototype at IIT Hyderabad

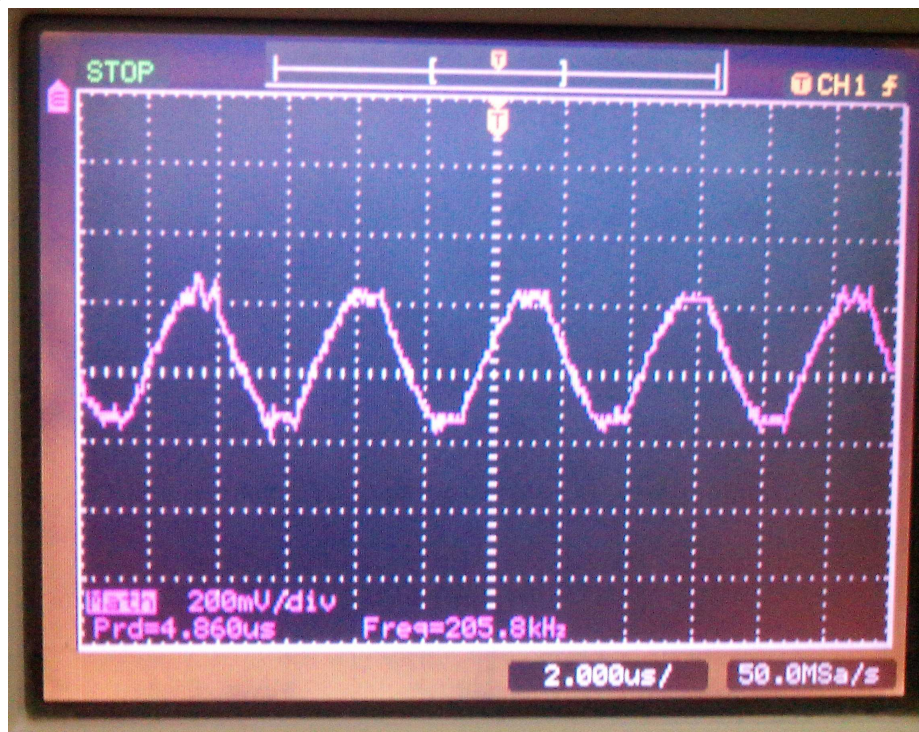


Figure 6.10: Modulated signal generated from the developed hardware prototype at IIT Hyderabad after low pass filter

Chapter 7

Conclusion

The study mainly focusses on the development of a smart and intelligent architecture for IoT enabled remote health monitoring applications. We proposed a rule engine based smart transmission scenario where the collected data is transmitted intelligently. Performance analysis of the proposed rule engine based smart transmission shows that it can aid for a significant energy savings and reduction in network traffic. We also proposed an on-chip context predictor based smart sensing technique which reduces the total amount of data generated by sensing the biological parameters intelligently. Performance of the on-chip context predictor based smart sensing technique is evaluated using mean deviation, duty cycle and energy savings as key parameters. The analysis shows that the proposed sensing mechanism achieves 72 % reduction in the system duty cycle and reduction in energy savings.

We analyzed the noise performance of IEEE 802.15.4-PHY along with three different pulse shaping techniques namely Raised Cosine, Root-Raised Cosine, Half-Sine pulse shaping. The analysis shows that the performance of root-raised cosine pulse shaping dominates the rest of the two pulse shaping techniques. Upon combining the pulse shaping with IEEE 802.15.4 standard specified DSSS, the performance is degraded than O-QPSK system without spreading and pulse shaping. We also discussed a modied IEEE 802.15.4-PHY, which uses Raised Cosine pulse shaping and whose performance is similar to IEEE 802.15.4-PHY with Half Sine pulse shaping at low SNRs. The modified IEEE 802.15.4-PHY when used along with IEEE 802.11b can significantly aid for design reuse of pulse shaping filter, thereby achieving multiplexed architecture and area optimization in on-chip multiple radios.

we also proposed a low complex mixer less QPSK based transmitter architecture using BJTs as primary elements in the analog bank which can greatly aid for IoT and M2M applications where the less design complexity is an important aspect. The architecture can also be developed using the MOSFET technology, with minor changes in the functional units of the architecture. A hardware prototype for the architecture proposed is developed in IIT Hyderabad and the generated modulated signal at a center frequency of 205.8 KHz has been analyzed. The quality of the modulated signal mainly depends on the quality of the signal generated by the memory unit. Lesser the distortion at the output of the memory unit, greater the quality of the modulated signal. The prototype developed is of low complex due to the elimination of mixers in the design. The other advantages of the proposed architecture are the ease of integration between digital functional units and the simple analog bank. The prototype developed at IIT Hyderabad has been successfully tested for generation

of various frequencies ranging from 1 KHz to 120 MHz. With the enhancement of technology, even higher frequencies upto GHz range can be generated.

Our future scope of the work is to explore the architecture multiplexing aspects among multiple on-chip raidos such as ZigBee, WiFi and Bluetooth LE for low complex hardware design.

List of publications

- Kiran, M.P.R.S.; Rajalakshmi, P.; Bharadwaj, K.; Acharyya, A., "Adaptive rule engine based IoT enabled remote health care data acquisition and smart transmission system," *Internet of Things (WF-IoT), 2014 IEEE World Forum on*, vol., no., pp.253,258, 6-8 March 2014
- Kiran, M.P.R.S.; Rajalakshmi, P.; Acharyya, A., Context Predictor Based Sparse Sensing Technique and Smart Transmission Architecture for IoT Enabled Remote Health Monitoring Applications. *36th Annual International Conference of the IEEE Engineering in Medicine and Biology Society*, 26-30 August 2014.
- Chivukula. K. B.; Vemishetty. N.; Sandeep Tiwari.; Kiran, M.P.R.S.; Acharyya, A.; Rajalakshmi, P.; Puddu, P.E., An Onchip Robust Real-time Automated Non-invasive Cardiac Remote Health Monitoring Methodology *41st annual international conference of Computing in Cardiology*, 7-10 September 2014. (Accepted)
- Kiran, M.P.R.S.; Jagadish, B.; Rajalakshmi, P., IoT Enabled Communication Device with Mixer Less Low Complex QPSK Based Transmitter Architecture for Low Frequency Applications, *17th International Symposium on Wireless Personal Multimedia Communications*, 7-10 September

References

- [1] IEEE Standard for Local and Metropolitan Area Networks-Part 15.4: Low-Rate Wireless Personal Area Networks (LR-WPANs), IEEE Computer Society Std.
- [2] Sahandi, R.; Yuanlong Liu, "Channel Overlap Problems of ZigBee Networks for Remote Patient Monitoring on General Hospital Wards," *Communications and Mobile Computing (CMC), 2010 International Conference on*, vol.3, no., pp.259,263, 12-14 April 2010
- [3] Borromeo, S.; Rodriguez-Sanchez, C.; Machado, F.; Hernandez-Tamames, J.A.; de La Prieta, R., "A Reconfigurable, Wearable, Wireless ECG System," *Engineering in Medicine and Biology Society, 2007. EMBS 2007. 29th Annual International Conference of the IEEE* , vol., no., pp.1659,1662, 22-26 Aug. 2007
- [4] Yu Meng; Dunham, M.H.; Marchetti, F.M.; Jie Huang, "Rare Event Detection in a Spatiotemporal Environment," *Granular Computing, 2006 IEEE International Conference on* , vol., no., pp.629,634, 10-12 May 2006
- [5] Rehunathan, D.; Bhatti, S.; Chandran, O.; Pan Hui, "vNurse: Using virtualisation on mobile phones for remote health monitoring," *e-Health Networking Applications and Services (Healthcom), 2011 13th IEEE International Conference on* , pp.82,85, 13-15 June 2011
- [6] Chowdhury, M.A.; McIver, W.; Light, J., "Data association in remote health monitoring systems," *Communications Magazine, IEEE* , vol.50, no.6, pp.144,149, June 2012
- [7] Priya, B.; Rajendran, S.; Bala, R.; Gobbi, R., "Remote wireless health monitoring systems," *Innovative Technologies in Intelligent Systems and Industrial Applications, 2009. CITISIA 2009* , vol., no., pp.383,388, 25-26 July 2009
- [8] www.meds.queensu.ca/central/modules/ECG/normalLecg.html
- [9] <http://gigaom.com/2011/10/13/internet-of-things-will-have-24-billion-devices-by-2020/>
- [10] The Mobile Economy, GSMA, 2013.
- [11] Abdul Qayoon Bhat, Vineet kumar, Sunil Kumar, "Design of ECG Data Acquisition System," *International Journal of Advanced Research in Computer Science and Software Engineering*, vol. 3, issue 4, April 2013.

- [12] S. Maheshwari, A. Acharyya, P. Rajalakshmi, P. E. Puddu and M. Schiariti (2013), "Accurate and Reliable 3-Lead to 12-Lead ECG Reconstruction Methodology for Remote Health Monitoring Applications," *IEEE International Conference on e-Health Networking, Applications and Services (Healthcom, 2013)*, 9-12 October, 2013, Portugal, 2013
- [13] GALEN S. WAGNER, Henry J. L. Marriot, "Marriott's Practical Electrocardiography".
- [14] Cuiwei Li; Chongxun Zheng; Changfeng Tai, "Detection of ECG characteristic points using wavelet transforms," *Biomedical Engineering, IEEE Transactions on* , vol.42, no.1, pp.21,28, Jan. 1995
- [15] L. Y. Di Marco, Lorenzo Chiari, "A wavelet-based ECG delineation algorithm for 32-bit integer online processing," *Biomedical Engineering online*, vol. 10, no. 2, article 23, 2011.
- [16] Pan, Jiapu; Tompkins, Willis J., "A Real-Time QRS Detection Algorithm," *Biomedical Engineering, IEEE Transactions on* , vol.BME-32, no.3, pp.230,236, March 1985.
- [17] Mazomenos, E.B.; Biswas, D.; Acharyya, A.; Chen, T.; Maharatna, K.; Rosengarten, J.; Morgan, J.; Curzen, N., "A Low-Complexity ECG Feature Extraction Algorithm for Mobile Healthcare Applications," *Biomedical and Health Informatics, IEEE Journal of* , vol.17, no.2, pp.459,469, March 2013
- [18] Mazomenos, E.B.; Chen, T.; Acharyya, A.; Bhattacharya, A.; Rosengarten, J.; Maharatna, K., "A Time-Domain Morphology and Gradient based algorithm for ECG feature extraction," *Industrial Technology (ICIT), 2012 IEEE International Conference on* , vol., no., pp.117,122, 19-21 March 2012
- [19] H. Zhou, D. Luo, Y. Gao and D. Zuo, "Modeling of Node Energy Consumption for Wireless Sensor Networks," *Wireless Sensor Network*, Vol. 3 No. 1, 2011, pp. 18-23. doi: 10.4236/wsn.2011.31003.
- [20] Goldberger AL, Amaral LAN, Glass L, Hausdorff JM, Ivanov PCh, Mark RG, Mietus JE, Moody GB, Peng C-K, Stanley HE. PhysioBank, PhysioToolkit, and PhysioNet: Components of a New Research Resource for Complex Physiologic Signals. *Circulation* 101(23):e215-e220 [Circulation Electronic Pages; <http://circ.ahaajournals.org/cgi/content/full/101/23/e215>]; 2000 (June 13).
- [21] Bousseljot R, Kreiseler D, Schnabel, A. Nutzung der EKG-Signaldatenbank CARDIODAT der PTB ber das Internet. *Biomedizinische Technik, Band 40, Ergnzungsband 1* (1995) S 317
- [22] Ian F. Akyildiz, Mehmet Can Vuran, "Wireless Sensor Networks"
- [23] Bio medical signal processing by D.C Reddy, principles and techniques, first edition. P 256,260
- [24] Candes, E.J.; Wakin, M.B., "An Introduction To Compressive Sampling," *Signal Processing Magazine, IEEE* , vol.25, no.2, pp.21,30, March 2008
- [25] Kiran, M.P.R.S.; Rajalakshmi, P.; Bharadwaj, K.; Acharyya, A., "Adaptive rule engine based IoT enabled remote health care data acquisition and smart transmission system," *Internet of Things (WF-IoT), 2014 IEEE World Forum on* , vol., no., pp.253,258, 6-8 March 2014

- [26] T.B. Parkin, S.T. Chester and J.A. Robinson, "Calculating Confidence Intervals for the Mean of a Lognormallaly Distributed Variable," vol. 54, no. 321?326, 1990.
- [27] C. E. Land, "Confidence Intervals for Linear Functions of the Normal Mean and Variance," *Annals of mathematical Statistics*, vol. 42, no. 4, pp. 1187-1205, 1971.
- [28] Goldberger AL, Amaral LAN, Glass L, Hausdorff JM, Ivanov PCh, Mark RG, Mietus JE, Moody GB, Peng C-K, Stanley HE. PhysioBank, PhysioToolkit, and PhysioNet: Components of a New Research Resource for Complex Physiologic Signals. *Circulation* 101(23):e215-e220 [Circulation Electronic Pages; <http://circ.ahajournals.org/cgi/content/full/101/23/e215>]; 2000 (June 13).
- [29] Bousseljot R, Kreiseler D, Schnabel, A. Nutzung der EKG-Signaldatenbank CARDIODAT der PTB ber das Internet. *Biomedizinische Technik, Band 40, Ergänzungsband 1 (1995) S 317*
- [30] Kuhn, J.A.; Alessi, R.V., "Mixed signal ASIC design issues and methodologies," *ASIC Seminar and Exhibit, 1989. Proceedings., Second Annual IEEE*, pp.T4, 1/1-9, 25-28 Sep 1989.
- [31] "Smart buildings: people and performance", *Royal Academy of Engineering*.
- [32] Dongjun Shen; Zhiqun Li, "A 2.4 GHz low power folded down-conversion quadrature mixer in 0.18- μ m CMOS," *International Conference on Wireless Communications and Signal Processing (WCSP)*, 2011, pp.1,4, 9-11 Nov. 2011.
- [33] Hanil Lee; Mohammadi, S., "A 500W 2.4GHz CMOS Subthreshold Mixer for Ultra Low Power Applications," *Radio Frequency Integrated Circuits (RFIC) Symposium, 2007 IEEE* , pp.325,328, 3-5 June 2007.
- [34] Memon, T.D.; Ghangro, W.; Chowdhry, B. S.; Shaikh, A.A., "Quadrature Phase Shift Keying modulator & demodulator for Wireless Modem," *Computer, Control and Communication, 2009. IC4 2009. 2nd International Conference on* , vol., no., pp.1,6, 17-18 Feb. 2009
- [35] S. Haykin, "Communication Systems", Third Edition, Wiley, 1994.
- [36] Santana Gomez, D.; Aguirre-Hernandez, I.A.; Rodriguez-Guarneros, Y.L., "PSK Digital Modulation DSP Implementation Applied to Software Radio," *Electronics, Robotics and Automotive Mechanics Conference, 2006* , vol.2, pp.106,109, Sept. 2006.
- [37] John G. Proakis, "Digital Communications", Fourth Edition, McGraw-Hill.
- [38] Standard[online]. Available: <http://pdf.datasheetcatalog.com/datasheet/SGSThompsonMicroelectronics/mXyzyyw.pdf>
- [39] Standard[online]. Available: <http://www.futurlec.com/Transistors/2N3702.shtml>
- [40] 1905.1-2013 - IEEE Standard for a Convergent Digital Home Network for Heterogeneous Technologies.
- [41] Peizhong Yi; Iwayemi, A.; Chi Zhou, "Developing ZigBee Deployment Guideline Under WiFi Interference for Smart Grid Applications," *Smart Grid, IEEE Transactions on* , vol.2, no.1, pp.110,120, March 2011.

- [42] Howitt, I. and Gutierrez, J.A. IEEE 802.15.4 low rate-wireless personal area network coexistence issues, *Wireless Communications and Networking*, 2003. WCNC 2003. IEEE, Volume: 3, 16-20 March 2003.
- [43] K. Shuaib, M. Alnuaimi, M. Boulmalf, I. Jawhar, F. Sallabi, and A. Lakas, Performance evaluation of IEEE 802.15.4: Experimental and simulation results, *J. Commun.*, vol. 2, no. 4, pp. 2937, Jun. 2007.
- [44] Bijaya Kumar Muni, Sarat Kumar Patra, Low Bit Error Rate ZigBee Baseband Transceiver Design for IEEE 802.15.4 ,” *MECON-2013, Amity university, NOIDA.*
- [45] Yao Liu; Peng Ning; Huaiyu Dai; An Liu, ”Randomized Differential DSSS: Jamming-Resistant Wireless Broadcast Communication,” *INFOCOM, 2010 Proceedings IEEE* , vol., no., pp.1,9, 14-19 March 2010
- [46] Fei Shang; Ben-qing Gao; Ge Liu; Xuan Xiao, ”Bit error performance analysis of FH/MSK system in different multi-tone noise jamming,” *Microwave, Antenna, Propagation and EMC Technologies for Wireless Communications, 2005. MAPE 2005. IEEE International Symposium on* , vol.2, no., pp.1398,1401 Vol. 2, 8-12 Aug. 2005
- [47] Da Gang Xie; Nan Wu; Chun Wang; Qi Feng Liu, ”Performance analysis and simulation of DSSS in tactical data link communication system,” *Environmental Electromagnetics (CEEM), 2012 6th Asia-Pacific Conference on* , vol., no., pp.194,197, 6-9 Nov. 2012
- [48] Salt, J.E.; Kumar, S., ”Suitability of MSK modulation in a direct-sequence spread spectrum system,” *Personal, Indoor and Mobile Radio Communications, 1992. Proceedings, PIMRC '92., Third IEEE International Symposium on* , vol., no., pp.610,617, 19-21 Oct 1992.
- [49] Jun Sang Han; Myoung Jin Kim, ”Offset Quadrature-Quadrature Phase Shift Keying with Half-Sine Pulse Shaping,” *ICT Convergence (ICTC), 2013 International Conference on* , vol., no., pp.931,935, 14-16 Oct. 2013.
- [50] Pal, M.; Pal, S., ”Analysis of performance of QAM system when subjected to sharpened Raised Cosine filter,” *Computers and Devices for Communication (CODEC), 2012 5th International Conference on* , vol., no., pp.1,4, 17-19 Dec. 2012.
- [51] Chia-Yu Yao; Chiang-Ju Chien, ”Design of a square-root-raised-cosine FIR filter by a recursive method,” *Circuits and Systems, 2005. ISCAS 2005. IEEE International Symposium on* , vol., no., pp.512,515 Vol. 1, 23-26 May 2005.